Lifespan Regulation by Insulin Signaling Through Phosphorylation of Proteins Beyond FOXO

Wen-jun Li
National Institute of Biological Sciences, Beijing
Li Tao
National Institute of Biological Sciences, Beijing
Chenwei wang
Huazhong University of Science and Technology
Yong-Hong Yan
National Institute of Biological Sciences, Beijing
Mei-Jun Zhang
National Institute of Biological Sciences, Beijing
Ze-Xian Liu
State Key Laboratory of Oncology in South China, Collaborative Innovation Center for Cancer Medicine, Sun Yat-sen University Cancer Center https://orcid.org/0000-0001-9698-0610
Yu-Xin Li
National Institute of Biological Sciences, Beijing
Hanqing Zhao
National Institute of Biological Sciences
Xue-Mei Li
National Institute of Biological Sciences, Beijing
Xian-Dong He
National Institute of Biological Sciences, Beijing
Yu Xue
Huazhong University of Science and Technology https://orcid.org/0000-0002-9403-6869
Meng-Qiu Dong (dongmengqiu@nibs.ac.cn)
National Institute of Biological Sciences https://orcid.org/0000-0002-6094-1182

Article

Keywords: Kinases-substrate Analysis, Proteomic Analysis, Machine Learning

Posted Date: October 2nd, 2020

DOI: https://doi.org/10.21203/rs.3.rs-72001/v1

Version of Record: A version of this preprint was published at Nature Communications on July 27th, 2021. See the published version at https://doi.org/10.1038/s41467-021-24816-z.

Abstract

Insulin/IGF-1 Signaling (IIS) constrains longevity by inhibiting the transcription factor FOXO. Beyond FOXO, little is known about how phosphorylation—as mediated by IIS kinases— regulates lifespan. Here, we profiled IIS-dependent phosphorylation changes in a large-scale quantitative phosphoproteomic analysis of wild-type and three IIS mutant *C. elegans* strains. Our state-of-the-art analysis experimentally identified more than 15,000 phosphosites, among which 448 were differentially phosphorylated in the long-lived *daf-2/insulin receptor* mutant. We developed a machine-learning-based tool for systematically ranking the likely functional importance of phosphosites to guide candidate selection for follow-up validation. We show that AKT-1 pT492 inhibits DAF-16/FOXO and compensates the loss of *daf-2* function, that EIF-2α pS49 potently regulates protein synthesis and *daf-2* longevity, and that reduced phosphorylation of multiple germline proteins (*e.g.*, CDK-1) apparently transmits a signal representing reduced DAF-2 signaling to the soma. Finally, kinase-substrate analysis and subsequent experimental validation confirm that casein kinase 2 negatively regulates lifespan. Our new benchmark data resource and machine-learning tool enables unprecedented access to detailed functional insights for studies of longevity.

Introduction

Despite the great diversity of lifespan in the animal kingdom, ancient genetic pathways have been found to regulate lifespan across species[1, 2]. The best-known example is Insulin/Insulin Growth Factor 1 (IGF-1) signaling (IIS). Polymorphisms of the component genes of this pathway are tightly associated with human longevity[2]. Disrupted IIS can extend lifespan up to ten fold in *C. elegans*[3]. The canonical IIS pathway of the worm comprises insulin-like ligands, the insulin/IGF-1 receptor tyrosine kinase DAF-2, the phosphatidylinositol-3-OH kinase (PI3K) AGE-1, the serine/threonine kinases PDK-1, AKT-1, and AKT-2, and a downstream transcription factor (TF) DAF-16, the *C. elegans* homolog of human FOXO[4]. Inhibiting the IIS kinases leads to nuclear translocation of DAF-16, subsequent activation of target gene transcription, and ultimately lifespan extension. While DAF-16 and other TFs are required for IIS-mediated lifespan extension[4], it has not been demonstrated that activation of TFs and the subsequent regulation at transcriptional level is sufficient for *daf-2* longevity.

Deep profiling of the *C. elegans* transcriptomes and proteomes made clear that age-dependent protein abundance changes correlated poorly with mRNA abundance changes[5, 6]. Similarly, for a significant subset of proteins that are up- or down-regulated in the long-lived *daf-2* mutant worms, there were no corresponding changes in the abundance of their mRNA templates. These changes affect known lifespan modulators such as components of translational machinery[7, 8, 9], indicating that post-transcriptional regulation does impact lifespan control.

Phosphorylation modification, among various post-transcriptional regulation, is understood as the fundamental regulatory mechanism underlying insulin/IGF-1 signal transduction. The IIS kinases AKT-1 and AKT-2 prevent lifespan extension by sequestering DAF-16 in the cytoplasm. Other kinases such as

JNK-1/JNK, CST-1/MST1, and AAK-2/AMPK contribute to *daf-2* longevity partly by promoting nuclear translocation of DAF-16[4]. All those kinases directly phosphorylate DAF-16 in vitro, yet such phosphorylation-based regulation has not been confirmed in vivo. *daf-2* longevity is also modulated by protein phosphatases: PPTR-1, a regulatory subunit of PP2A, reduces the phosphorylation of AKT-1 T350, and renders AKT-1 less active[10]; $PP4^{SMK-1}$ dephosphorylates the transcriptional regulator SPT-5/SUPT5H, which facilitates DAF-16 activity in *daf-2* worms[11]. To our knowledge, very few studies have reported phosphosites which regulate lifespan[12, 13, 14, 15, 16], and there are no reports of large-scale survey studies of *C. elegans* IIS-related phosphorylation.

To date, 119,809 phosphorylation sites on human proteins have been identified; the number for *C. elegans* is only 10,767[17, 18]. The paucity of data in *C. elegans* reflects the fact that *C. elegans* – traditionally a genetic system – has fallen seriously behind, even though mass spectrometry (MS) -based phosphoproteomics technologies have been leaping forward. Here, using the state-of-the-art phosphoproteomics technology, we surveyed the landscape of protein phosphorylation in *C. elegans* and compared through a ^{15}N-labled reference sample the long-lived *daf-2* mutant worms to the wild type, the *daf-16* mutant, and the *daf-16; daf-2* double mutant. This led to the identification of over 15,000 phosphosites, a doubling of the *C. elegans* phosphorylation database, and the discovery of 448 phosphosites regulated by IIS. Further, we developed a machine learning based algorithm to identify phosphosites that likely exert biological impacts. This tool guided our functional investigations of three phosphosites, all of which do impact worm lifespan. Briefly, we added a new element – phosphorylation of AKT-1 T492 – to the negative feedback regulation mechanism of IIS. We also uncovered two branches of signaling downstream of DAF-2 that extend lifespan: inhibition of translation through phosphorylation of EIF-2α S49 by GCN-2 and signaling in the germline through phosphorylation of CDK-1 T179. Lastly, global enrichment analysis and subsequent validation experiments highlighted the germline as a target tissue of IIS and revealed a role for casein kinase 2 in lifespan determination.

Results

Profiling the *C. elegans* Phosphoproteome by MS in Advanced Approach

The phosphoproteome of *C. elegans* has not been surveyed rigorously; seeking to increase the coverage of the *C. elegans* phosphoproteome while aiming for high accuracy in both identification and quantification of phosphopeptides, we combined a number of technical elements and optimized the analytical workflow (Fig. 1A). These technical elements include extensive high-pH reverse phase fractionation coupled with interval pooling[19, 20], polyMAC-Ti enrichment of phosphopeptides[21, 22], high-speed and accurate-mass mass spectrometry, and stable isotope (^{15}N) metabolic labeling, a highly accurate quantitative proteomics strategy (Fig. 1A).

From wild type (WT) *C. elegans* and the insulin signaling mutants (*daf-2*, *daf-16*, and the *daf-16; daf-2* double mutant) — each analyzed in three or four biological replicates and two technical replicates — we

identified a total of 15,443 phosphorylation sites with > 0.75 PhosphoRS site probability[23]. These phosphosites are represented by 22,536 phosphopeptides or 15,723 phosphoisoforms that belong to 4,418 proteins (Supplementary Fig. 1A-C). 9,949 phosphosites identified in this study are not covered by dbPAF, which is a comprehensive database dedicated to collecting phosphosites in humans, animals, and fungi[17]. Notably, the addition of these newly identified phosphosites close to doubles the current collection for *C. elegans* (Fig. 1B).

Although it is well established that phosphorylation is the primary means by which the IIS pathway transmits signals, very little is known about which sites are phosphorylated, even for the core components of *C. elegans* IIS. For example, dbPAF presently contains no phosphosites for the PI-3 kinase AGE-1. Here, our phosphoproteomics analysis uncovered 32 phosphosites in ten *C. elegans* IIS proteins, 17 of which have not been previously reported (Fig. 1C). These new, high confidence phosphosites (Fig. 1C, dark blue) are distributed throughout the pathway, from the upstream insulin-like ligands to the downstream FOXO transcription factor DAF-16, and for every kinase in between.

More than 15,000 phosphopeptides were quantified against their ^{15}N-labeled cognate peptides, which were introduced as an internal reference standard by feeding *C. elegans* entirely on ^{15}N-labeled bacteria (Supplementary Fig. 1B, see Methods). These peptides represent 10,705 quantifiable phosphoisoforms (Fig. 1D, Supplementary Fig. 1B-C, and Supplementary Table 1), about a quarter of which carry combinatorial information for two or more phosphosites. Clustering analysis of their abundance levels (relative to ^{15}N-labeled peptides) across WT and IIS mutants indicated that the *daf-2* mutant samples are clearly different from the WT, the *daf-16*, and *daf-16; daf-2* samples. In other words, the quantitative phosphoproteomics data clustered according to the lifespan phenotype, not by batch (Supplementary Fig. 1E). The Spearman correlation coefficient between biological replicates of the same worm strain is in the range of 0.70–0.91. These results are indicative of high data quality for phosphopeptide identification and quantification.

Phosphorylation Changes Resulting from Genetic Disruption of IIS

Disrupting the activity of IIS induced abundance changes on 501 phosphoisoforms (> 1.5-fold in at least one of the IIS mutants relative to WT, Supplementary Fig. 1F). As expected, clustering and pathway enrichment analysis show that phosphorylation on proteins involved in FOXO signaling and longevity regulation were down-regulated in the *daf-2* mutant. We also found that proteins related to protein synthesis or degradation had lower phosphorylation levels in the *daf-2* mutant, but the changes were not preserved in the *daf-16* or *daf-16; daf-2* mutants. Notably, glycerolipid metabolism and glycerophospholipid metabolism were enriched for proteins with up-regulated phosphorylation in the *daf-2* mutant. Up-regulation of lipid metabolism is a major phenotype of *daf-2* mutants[4, 24]. Underlying this phenotype are gene expression changes[25, 26] and protein abundance changes [8]. Thus, our results should be highly informative in supporting characterization of biological processes regulated by IIS and are likely to extend the existing mechanistic understanding of this field to encompass PTM-level regulation.

Development of a Computational Strategy to Prioritize Putative Functional Phosphosites

A bottleneck in present-day biomedical research is a lack of efficient methods for extracting useful information from omics data[27, 28]. To facilitate the translation of phosphoproteomics data into biological insights, we developed a machine learning based method named iFPS (Inference of Functional Phosphorylation Sites) to predict whether a given phosphosite likely exerts a biological impact (Fig. 2A). Although the lack of suitable training data has to date prevented development of such a tool in *C. elegans*, note that a tool for similar predictive analysis of phosphorylation sites recently became available for *Homo sapiens*[18]. Our iFPS tool assesses six types of constraints for each phosphosite under examination (Supplementary Fig. 2A-H, see Methods), including 1) how many kinase families have consensus substrate sites that match its sequence context?; 2) how evolutionarily conserved a phosphosite is; 3) how many interacting domains are predicted to be influenced by phosphorylation at this site, 4) occurrence of a predicted acetylation site near the phosphosite (which could engage in PTM crosstalk); 5) relative surface accessibility; and 6) predicted secondary structure of the peptide containing the phosphosite.

For the initial iFPS training data, we searched in the literature for *C. elegans* phosphosites whose functions have been experimentally validated: the resulting 121 functional phosphosites served as the original positive training data set (Supplementary Table 2). The negative data set contained 605 (121 × 5) randomly selected phosphosites from dbPAF. Multinomial logistic regression (MLR), a widely used machine learning algorithm, was adopted for training the computational models, and 10-fold cross-validations were performed. The final model was determined automatically, and the highest area under the curve (AUC) value was 0.88 (Supplementary Fig. 2I). iFPS was applied to score all phosphosites identified in this study, which contain 31 known functional phosphosites from the positive data set (Supplementary Table 2). Distributions of iFPS scores show that functionally impactful phosphosites ranked higher than other phosphosites (Fig. 2B). Half of the functional phosphosites were among the top 5% iFPS scoring list.

Next, we focused on putative functional phosphosites regulated by *daf-2*. From the quantitation data reliability measured at least three times in both the *daf-2* mutant and a control (WT or WT plus *daf-16* mutants, see Methods), we found 222 down- and 226 up-regulated phosphoisoforms upon reduction of *daf-2* activity (Fig. 2C). By overlapping the phosphosites regulated by *daf-2* and the top 5% highest scoring iFPS phosphosites (Supplementary Table 2–3), we identified 27 high-priority phosphosites (*i.e.*, with a high probability of being functionally impactful) (Fig. 2D). Notably, these sites do not represent a random set: the majority of the parent proteins harboring these sites function in either AMPK/insulin signaling, translation initiation/ribosome biogenesis, or cell cycle regulation. Further, 13 out of the 27 high-priority phosphosites are from eight proteins (AAK-2, AKT-1, CDK-1, DAF-16, EGL-45, MLT-3, MVK-1 and PDHA-1) known to regulate lifespan (phenotypic data from WormBase release WS275). Of note, the phosphorylation state of three conserved S/T residues of AAK-2, the catalytic subunit of *C. elegans* AMPK, was differentially regulated in the *daf-2* mutant: phosphorylation of T597 and S601 increased whereas S553 decreased.

Any function(s) for most of the high-priority phosphorylation sites remain uncharacterized. In lifespan regulation, only S345 of DAF-16, a conserved AKT site, has been implicated: simultaneous mutation of S345 and other three predicted AKT sites induced nuclear accumulation of DAF-16, much like in the *daf-2* mutant but without the extraordinary longevity phenotype[13]. To experimentally test the performance of iFPS and to flesh out the mechanism of lifespan extension by protein phosphorylation in response to reduced insulin signaling, we focused on several phosphosites for in-depth functional analysis (colored red in Fig. 2D). These are AKT-1 T492, EIF-2α S49, and CDK-1 T179, one in each of the three prominent protein function groups.

Constitutive Phosphorylation of AKT-1 T492 Promotes AKT-1 Activity

iFPS prioritized pT492 of worm AKT-1 (corresponding to pT450 of human AKT-1) (Fig. 3A). This site is positioned in a highly conserved turn motif near the AKT-1 C-terminus, and work in mammalian cells has shown that this site is co-translationally phosphorylated by mTORC2, supporting that this site may stabilize newly synthesized AKT[29, 30]. However, the functional impact of this site has not been confirmed.

Verifying the earlier suggestion, we found that phosphorylation of *C. elegans* AKT-1 on T492 is constitutive. The AKT-1 protein and T492 phosphorylation levels both doubled in the long-lived *daf-2* mutant (FC = 2.2–2.4, *daf-2*/WT) as measured by shotgun proteomics (Fig. 2D and Supplementary Table 3) and by targeted quantitation assays using synthesized peptides bearing isotope labels (Fig. 3B). Whereas the T492-containing peptide of AKT-1 was undetectable in any of the four strains analyzed (Fig. 3B), the pT492-containing peptide of AKT-1 was readily detectable, and its abundance change followed that of the AKT-1 protein very closely. Thus, the T492 site is apparently constitutively phosphorylated following ATK-1 translation.

We used CRISPR/Cas9 to produce a T492A AKT-1 variant. Compared to the WT worms, those expressing the non-phosphorylatable T492A AKT-1 variant exhibited diverse phenotypes: *akt-1-T492A* mutant worms resembled weak IIS loss-of-function mutants such as *akt-1(lf)* or weak alleles of *daf-2(lf)*. AKT-1-T492A caused nuclear accumulation of DAF-16::GFP in the intestinal cells of nearly 60% of worms, representing a 6-fold increase from the 9% detected in the WT animals (Fig. 3C) and indicating that phosphorylation of T492 promotes AKT-1's ability to phosphorylate and thereby inhibit DAF-16. Consistently, the T492A mutation moderately but significantly extended the lifespan of WT worms by 8–17% (Fig. 3D), comparable to the 8–21% increase in lifespan conferred by the *akt-1(lf)* allele[31]. Notably, the pro-dauer formation effect of AKT-1-T492A is less obvious in *akt-1(null)*: it failed to induce dauers at 27 °C. However, the T492A mutation did enhance the dauer formation phenotype in the sensitized background of *daf-2(e1370)* at 21 °C (Supplementary Fig. 3A).

To determine whether the loss-of-function phenotypes resulting from the T492A mutation are caused by destabilization of AKT-1, we used a knock-in approach to fuse a GFP reporter C-terminal to AKT-1. AKT-1::GFP and AKT-1-T492A::GFP were present in nearly all examined tissues, with no discernable difference in GFP intensity (Supplementary Fig. 3B-C), suggesting that T492A imparts no or little destabilizing effect

on AKT-1. However, we did observe an effect related to the subcellular localization of AKT-1. Compared with AKT-1::GFP, there is more AKT-1-T492A::GFP in the nuclei of oocytes (Supplementary Fig. 3D). This T492A-induced localization change for AKT-1 was limited to the germline, and had high penetrance (84%). Moreover, this phenotype does not result from an overexpression artifact, because both AKT-1::GFP and AKT-1-T492A::GFP are expressed from the edited endogenous *akt-1* gene locus. Since AKT-1 is normally recruited to the plasma membrane —where it transmits signals from receptor tyrosine kinases such as DAF-2—the nuclear translocation of AKT-1 may partially account for the observed loss-of-function effect of the T492A mutation. These results support that mutation of T492 to alanine impairs the activity of AKT-1, weakening AKT-1's inhibition of DAF-16 and leading to both longer lifespan and a higher propensity for dauer formation. Thus, in WT animals, constitutive phosphorylation of T492 promotes the kinase activity of AKT-1.

AKT-1 is controlled by a negative feedback loop at the gene transcription level; that is, expression of the *akt-1* gene is positively regulated by DAF-16[32], while DAF-16 itself is negatively regulated by AKT-1. In the long-lived *daf-2* mutant, activated DAF-16 induces transcription of *akt-1*, although the *akt-1* mRNA level is elevated by only 10%[33]. However, this elevation is strikingly higher when examined at the protein level: the AKT protein level is elevated by around 140% as measured by quantitative proteomics[6], a finding validated by our data for AKT-1::GFP in the present study (Supplementary Fig. 3E). Our phosphoproteomics analysis thus reveals T492 phosphorylation as a previously unknown layer of regulation in a complex regulatory network. Recalling that AKT-1 is phosphorylated at T492 immediately following its translation and that this PTM promotes AKT-1's activity, our work at the phosphoproteomics level underscores how a negative IIS feedback loop is intricately controlled at multiple regulatory layers, including gene transcription, protein synthesis, and post-translational modification (Fig. 3E).

EIF-2α pS49 Potently Regulates Protein Synthesis and Lifespan in the *daf-2* Mutant

Down-regulation of the processes that support protein synthesis (*e.g.*, translation initiation and ribosome biogenesis) has been associated with longevity in previous studies[34, 35, 36]. The same down-regulation trend was evident in our phosphoproteomics data: phosphorylation of multiple eukaryotic initiation factors (EIF) was generally reduced in the long-lived *daf-2* mutant (Supplementary Fig. 4A). The only exception to this trend was EIF-2α. Phosphorylation of EIF-2α at S49, which is an iFPS prioritized site, nearly doubled in the *daf-2* mutant relative to WT worms (Fig. 2D and 4A), and this was verified by western blotting (Fig. 4B).

C. elegans EIF-2α S49 is a highly conserved site and is equivalent to human eIF2α S51, whose phosphorylation is known to block global mRNA translation[37, 38]. We thus asked whether mRNA translation is suppressed in the *daf-2* mutant through hyper-phosphorylation of EIF-2α S49. We engineered an EIF-2α S49A mutation in the *C. elegans* genome using a CRISPR/Cas9 mediated gene editing method. Indeed, the S49A mutation, which locks EIF-2α in the dephosphorylation state, markedly increased the poly-ribosome fraction in the *daf-2* mutant, albeit short of restoring it to the WT level (Fig. 4C). Further, the EIF-2α S49A mutation, which had no effect on WT lifespan, suppressed *daf-2*

longevity by 30% (Fig. 4D). These results suggest that enhanced phosphorylation of EIF-2α S49 in the *daf-2* mutant may promote longevity by suppressing protein synthesis.

Next, we asked which kinase is responsible for hyper-phosphorylation of EIF-2α S49 in the *daf-2* mutant. Mammalian eIF2α S51 may be phosphorylated by PERK, GCN2, HRI, or PKR[38], among which only PERK and GCN2 have orthologs in *C. elegans*. We found that the *gcn-2(lf)* mutation significantly reduced EIF-2α S49 phosphorylation in the *daf-2* mutant, while deletion of *pek-1* had a weaker effect (Fig. 4E). Consistently, *gcn-2(lf)* suppressed *daf-2* longevity (Fig. 4D) whereas *pek-1(null)* did not (Supplementary Fig. 4B). Therefore, we conclude that the GCN-2 kinase is responsible for the increased phosphorylation of EIF-2α S49 we observed in the *daf-2* mutant and that GCN-2-mediated hyper-phosphorylation of EIF-2α S49 slows down protein synthesis in the *daf-2* mutant to delay ageing.

Of note, two lines of evidence suggest that phospho-EIF-2α has a potent effect. First, a tiny amount of EIF-2α pS49, so low that it was undetectable by MS unless the phosphopeptides were enriched beforehand, is sufficient to generate the protein synthesis and lifespan phenotype. The S49 containing peptide generated by trypsin digestion from endogenous EIF-2α was only detectable and quantifiable by MS in the non-phosphorylated form in whole worm lysate samples (Supplementary Fig. 4C-E). Second, overexpression or knock-in mutation of the phospho-mimic EIF-2α S49D/E is lethal, suggesting a strong dominant effect of EIF-2α S49 phosphorylation. These target quantitation and genetics results both support that EIF-2α S49 phosphorylation has a potent inhibitory effect on protein synthesis and contributes substantially to *daf-2* longevity (Fig. 4F).

Notably, our quantitative phosphoproteomics data also suggest that the observed EIF-2α pS49 increase of the *daf-2* mutant (*daf-2/*WT = 1.83) may occur independently of *daf-16*: the EIF-2α pS49 increase was still observed upon deletion of *daf-16* (*daf-2; daf-16/* WT = 1.91) (Supplementary Fig. 4F). Pursuing this, it was surprising when we found that among the 448 phosphoisoforms which were differentially regulated in the *daf-2* mutant (Fig. 2B), 124 apparently require *daf-16*, while 123 do not (Supplementary Table 3). This apparently very-well-balanced distribution of *daf-16* dependent vs. *daf-16* independent phosphorylation changes seems quite unique; to our knowledge, most of the documented changes in *daf-2(lf)* worms are dependent on *daf-16*. For example, two thirds or more of the protein abundance changes seen in the *daf-2* mutant were suppressed by *daf-16(lf)*[9].

Beyond EIF-2α, we characterized another EIF protein C37C3.2 (*C. elegans* eIF5). iFPS did not rank EIF-5 pT376 and pS380 among the top 5% (Supplementary Fig. 4G). The phosphorylation level of pS380 or pT376 pS380 either decreased or had no change, respectively, in the *daf-2* mutant (Supplementary Fig. 4G). Simultaneous mutation of EIF-5 T376 and S380 to T375A S380A (2A) or T375E S380E (2E) by CRISPR/Cas9 had no or little effect on WT lifespan, and did not alter the lifespan of *daf-2* (*e1370* or RNAi) worms (Supplementary Fig. 4H-I). These findings indicate that, at least in the context of insulin-signaling-mediated lifespan extension, the two phosphosites of EIF-5 are not functionally impactful. At minimum, this result helps validate the utility of iFPS ranking as a hypothesis-generating tool to efficiently inform prioritization of candidates for functional studies.

CDK-1 and Other Germline Phosphoproteins Contribute to Lifespan Determination

CDK-1 is a master regulator of the cell cycle. For *C. elegans* germ cell division, CDK-1 is specifically required for entry into the M phase[39]. iFPS prioritized worm CDK-1 pT32, pY33, and pT179 (Fig. 2D), which respectively correspond to human CDK1 pT14, pY15, and pT161, (Fig. 5A). CDK-1 activity is inhibited by phosphorylation of T14 and Y15 by WEE1/MYT1, but is activated by phosphorylation of T179 by CAK[40]. In the *daf-2* mutant, both inhibitory phosphorylation (pT32, pY33) and activating phosphorylation (pT161) of *C. elegans* CDK-1 decreased by 34–49%, while the CDK-1 protein level was about the same as that in WT worms (Fig. 5B).

Since the inactive form of CDK-1 (pT32 pY33) is not dominant negative, a reduced level of pT179 can be interpreted as a reduction of CDK-1 activity in the *daf-2* mutant. Note that interpretation is supported by elaborate study of the *daf-2* germline which reported a cell cycle delay in G2 in the proliferative zone; that is, proliferating *daf-2* germ cells are slow to enter the M phase[41]. Importantly, all of our phosphoproteomics samples were synchronized to adult day one—a stage at which germ cells are the only dividing cells— so we can confidently assume that any detected CDK-1 activity must come from the germline.

We then asked whether the reduction of CDK-1 pT179 or CDK-1 activity in the *daf-2* germline contributes to longevity. Mutating CDK-1 T179 to either A or E by gene editing was predictably unsuccessful: experimentally locking CDK-1 into either a completely inactive or a constitutively active state prevents cell cycle progression, causing lethality. We then took advantage of a temperature sensitive allele of c*dk-1(ne2257ts)* harboring an I173F mutation five amino acids away from T179 in the activation loop. We found that shifting *cdk-1(ne2257ts)* worms from the permissive temperature of 15 °C to the restrictive temperature 22.5 °C on adult day one significantly extended WT lifespan (by 11–30%), and noted that this extension was *daf-16* dependent (Fig. 5C). We also found that temperature-shift-induced inactivation of CDK-1(I173F) at earlier time points extended WT lifespan (Supplementary Fig. 5A). Likewise, we observed an extended lifespan of 20–30% upon knockdown of *cdk-1* starting from adult day one in the *rrf-1(pk1417)* mutant (in which RNAi is restricted in the germline, intestine, and some hypodermal cells[42]), whereas no extended lifespan phenotype resulted from intestine- or hypodermis-restricted *cdk-1* RNAi in these animals (Supplementary Table 4). These results support that reduced CDK-1 activity in the adult germline is sufficient to promote a moderate lifespan extension.

Next, we investigated whether reduced CDK-1 pT179 in the adult germline is necessary for lifespan extension upon DAF-2 depletion. Using both gene editing and auxin-induced protein degradation (AID) technologies[43], we were able to selectively degrade DAF-2 or WEE-1.3, or both, in the adult germline with high spatiotemporal precision. Degradation of WEE-1.3, the *C. elegans* ortholog of human WEE1/MYT1[40], should eliminate inhibitory phosphorylation of CDK1 on T32 and Y33 to drive an elevation of CDK-1 activity. Indeed, degrading WEE-1.3 specifically in the adult germline significantly shortened the lifespan of worms lacking germline DAF-2 (Fig. 5D). Moreover, both adult-specific and germline-specific degradation of DAF-2 slightly increased the mean lifespan and the maximal lifespan in two independent

experiments, but not in a statistically significant manner. We thus conclude that reduced CDK-1 pT179 in the adult germline may confer a small contribution to *daf-2* longevity.

It was highly striking that germline expression was predicted for the parent proteins of more than 70% of the iFPS-prioritized phosphosites (Supplementary Fig. 5B). Further, it was conspicuous that proteins of the reproductive system were highly enriched among the hypo-phosphorylated proteins detected in the long-lived *daf-2* mutant (Fig. 5E). These findings motivated us to conduct a small-scale RNAi screen in the *rrf-1(pk1417)* mutant background to explore how germline phosphoproteins may affect ageing of the soma (Supplementary Fig. 5C). Interestingly, we found that adult onset RNAi of genes that promote mitosis or meiosis generally extended lifespan, whereas RNAi of genes that limit the genesis of germ cells or gametes shortened lifespan (Fig. 5F and Supplementary Fig. 5C). These results are in line with reports of lifespan extension through germline ablation[44], and echo with the antagonistic pleiotropy theory of ageing. They also suggest that, although reduced CDK-1 pT179 alone contributes marginally to *daf-2* longevity, the phosphorylation changes among all germline proteins may collectively confer a sizable contribution to lifespan extension (Fig. 5G).

Reduction of Casein Kinase 2 (CK2) Activity Prolongs Lifespan

Based on the hyper- and hypo-phosphorylated sites we detected in the *daf-2* mutant, and in light of kinase-substrate relationships predicted with the iGPS algorithm[45], we explored which kinases are likely to be more or less active upon reduced insulin signaling. Specifically, we used hypergeometric tests followed by Benjamini-Hochberg adjustment to assess whether the predicted or potential substrate sites of a given kinase were enriched among the differentially regulated phosphoisoforms of the *daf-2* mutant. The hypo-phosphorylated sites displayed significant enrichment for putative substrate motifs (of 22 kinases), whereas no enrichment for kinase binding motifs was evident among the hyper-phosphorylated sites (Fig. 6A). There are studies for 5 of the 22 kinases reporting that RNAi or loss-of-function mutation extend lifespan (Fig. 6A), including investigations of *C. elegans* mTOR kinase LET-363 and the MAPK activated kinase MAK-2 and MNK-1.

Casein kinase 2 (aka CK2), was among the 22 kinases with a predicted activity decrease in the *daf-2* mutant. In fact, there were two kinase binding motifs in CK2 which were significantly overrepresented among the hypo-phosphorylated sites found in the *daf-2* mutant (Fig. 6B). Further implicating the likely impact of CK2 phospho-status in *daf-2* longevity, an motif-x analysis[46] detected CK2 but none of the 21 other kinases from our initial iGPS analysis. The *C. elegans* CK2 holoenzyme is composed of KIN-3, the catalytic subunit, and KIN-10, the regulatory subunit. CK2 has been shown to slow down ageing in *C. elegans*[47], but studies in yeast revealed an opposite effect, reporting that the *Saccharomyces cerevisiae* CK2 accelerates both chronological and replicative ageing[48, 49]. We examined the lifespans of worms treated variously with *kin-3* RNAi, *kin-10* RNAi, or the CK2 inhibitor TBB. *kin-3* or *kin-10* knockdown during adulthood moderately but significantly extended WT lifespan in four independent trials (Fig. 6C and Supplementary Table 4). More strikingly, 24 and 48-hour TBB treatment (from adult day one) extended

WT lifespan by 21–27% (Fig. 6D and Supplementary Table 4). These results demonstrate that inhibition of CK2 in young adults promotes longevity in *C. elegans*.

Discussion

Reducing the activity of IIS significantly extends lifespan and mobilizes deeply conserved lifespan modulators, primarily through phosphorylation. However, the in-depth mechanisms of lifespan regulation by IIS-related phosphorylation have been largely neglected. Also, technical challenges for large-scale characterization of functional phosphorylation sites have hindered the gathering of experimentally confirmed phosphosites. In the present study, we conducted a large-scale quantitative phosphoproteomics survey to address these issues. Our results dramatically increase the total number of in vivo phosphorylation sites in *C. elegans*. Moreover, by developing a machine learning based prioritization tool for prioritizing phosphosites for functional confirmation with extensive phosphosite-specific mutagenesis experiments, we offer multiple demonstrations for how functional phosphorylation events modulate signaling pathways to control lifespan regulation.

Extensive Phosphorylation Regulation Orchestrated by IIS Kinases Controls Lifespan Regulation

Previous studies investigating how reduced IIS extends lifespan have focused on transcriptional regulation by FOXO. While it is clear that DAF-16/FOXO activation is required for the long lifespan of the *daf-2* mutant, it is an open question whether DAF-16 activation is sufficient for *daf-2* longevity. Here, we looked into this issue by analyzing the phosphorylation changes against previously documented protein and mRNA abundance changes[6, 33]. We found lifespan-affecting phosphorylation changes at the three phosphorylation we characterized in-depth: AKT-1 pT492, EIF-2α pS49, and CDK-1 pT179 (Fig. 7). In particular, increased EIF-2α pS49 contributes significantly to *daf-2* longevity, and this regulation occurs specifically at the PTM level, not at the mRNA or protein level. Besides, hyper-phosphorylation of EIF-2α at S49 persisted in the *daf-16; daf-2* double mutant (Supplementary Fig. 4F and Supplementary Table 3), suggesting a *daf-16* independent change. GO terms related to cell cycle and translation were significantly enriched from phosphosites regulated by *daf-2* but independent of *daf-16*, whereas no enrichment was evident for *daf-16* dependent phosphosites. Importantly, our present study as well as previous evidences confirm that retarding the cell cycle or mRNA translation results in lifespan extension, indicating *daf-16*-independent phosphorylation events as IIS-related lifespan regulation mechanisms. Taken together, our phosphoproteomics and functional studies suggest that DAF-16 mediated transcriptional regulation alone may be insufficient for *daf-2* longevity.

Functional analysis results from this study indicate that the phosphoproteins from the reproductive system do affect lifespan; indeed, there are often negative correlations between the reproduction- and lifespan-related phenotypes upon mutating these phosphoproteins. Consider that adult-specific knockdown of genes including *cdk-1*, *chk-2*, *hoe-1*, *hsr-9*, and *htp-3* promotes cell cycle progression and results in lifespan extension, whereas early death phenotypes result from knockdown of the germline hyperproliferation suppressor *gld-1* or the oogenesis-restricting *puf-3*. These data endorse the

antagonistic pleiotropy theory, which proposes that ageing is an adaptation to natural selection of pleiotropic genes that benefit fitness in early life, but are detrimental later [50]. Assayed individually, these hypo-phosphorylated proteins of the reproductive system exhibit only small effects; however, we speculate that they may exert larger effects when combined. Notably, we did not detect clear patterns for mRNA- or protein-level changes for these phosphoproteins in the *daf-2* mutant (Fig. 7).

Regarding kinases with activities predicted to be reduced in the *daf-2* mutant, a survey of their lifespan phenotypes reported in the literature and our target analysis of the CK2 kinase KIN-3/KIN-10 suggests that, for the most part, their reduced activities contribute positively to *daf-2* longevity, with CST-1 being the only exception among seven studied kinases. As no clear pattern of changes is evident for these kinases in the *daf-2* mutant at the mRNA or protein-abundance levels (Fig. 7), our study underscores the utility of phosphoprotein-based surveys for elucidating the impacts of insulin signaling on longevity specifically and for deepening biological understanding generally.

EIF-2α Phosphorylation Links IIS-Modulated Amino Acid Metabolism to Translation and Longevity

The *daf-2(lf)* mutation led to reduced levels of ribosomal proteins and poly-ribosome associated RNAs, suggesting a repression of global mRNA translation. Previous studies reported that that *tts-1*, a long noncoding RNA, was required for the reduction of ribosome-associated RNA in *daf-2* worms[51]. We found here that GCN-2/EIF-2α phosphorylation signaling bridges translation and longevity in *daf-2* worms (Fig. 4F and 7). In eukaryotes, eIF2α phosphorylation converts eIF2-GDP into a competitive inhibitor of eIF2B, thus dominantly reducing pre-initiation complex assembly and general translation initiation[38]. Paradoxically, EIF-2α phosphorylation stimulates translation of *atf-5*, a transcription factor homologous to yeast GCN4 and mammalian ATF4[52]; phospho-eIF2α-induced ATF4 expression is required for tumor cell survival and embryonic stem cell proliferation[53, 54]. However, knocking out *atf-5* had no effect on the lifespan of WT or *daf-2* worms (Supplementary Table 4), indicating that the pro-longevity effect of EIF-2α phosphorylation mainly results from retarding general translation, rather than from promotion of ATF-5 translation. It remains to be clarified whether phospho-EIF-2α targets specific mRNA translation to promote lifespan. It is notable that EIF-2α S49A did not fully restore the peak heights of ribosomal fractions in *daf-2* (Fig. 4C), suggesting additional forms of regulation, for example *tts-1* associated ribosome reduction, is apparently involved.

The eIF2α kinases GCN2 and PERK are activated by amino acid depletion and ER stress, respectively. Our data suggest that GCN-2, not PEK-1, mediates the hyper-phosphorylation of EIF-2α S49 and promotes *daf-2* longevity. This is consistent with previous reports that *pek-1* null status neither abrogated ER stress resistance nor shortened the long lifespan of *daf-2* worms[55]. The next question is how the *daf-2* mutation activates GCN-2: several lines of evidence suggest that GCN-2 activity may respond to the IIS-modulated amino acid metabolism. First, uncharged tRNAs or ribosomal stalling directly stimulate GCN2 upon amino acid starvation[56, 57]. Also, knockdown of worm tRNA synthetases induces EIF-2α S49 phosphorylation through GCN-2[52]. Additionally, reduction of *daf-2* activity lowers the abundance of tRNA

synthetases and amino acid pools in young adult worms[7, 9, 58]. It therefore seems plausible that a shortage of tRNA synthetases and amino acids could lead to loss of tRNA charging and/or ribosome pausing, therefore stimulating GCN-2, a scenario that would support a role for GCN-2/EIF-2α signaling in altering amino acid metabolism to ameliorate translation and longevity in *daf-2* animals.

Germline Phosphoproteins Mediate the Effects of IIS on Reproduction and Lifespan Regulation

daf-2 and *daf-16* mainly function in neurons, the hypodermis, and intestine to regulate lifespan[26, 59, 60]. On the one hand, ablation of germline precursor cells further extends the lifespan of *daf-2* worms, suggesting that IIS acts in parallel with germline signaling to regulate lifespan[44]. On the other hand, IIS is required for germline cell cycle progression to ensure robust germline proliferation[41]. Recent data are starting to indicate a link (probably orchestrated by IIS-regulated SUMOylation) between lifespan regulation by germline signaling and IIS[61].

Here, we found that IIS actively induces phosphorylation on hundreds of germline proteins involved in the cell cycle, apoptosis, translation, etc., indicating pronounced functional impacts from phospho-modulation of germline proteins. As an example, we show that hypo-phosphorylated CDK-1 T179, which inactivates CDK-1 and thereby delays the cell cycle, potentially thereby contributing to *daf-2* longevity by transmitting a signal representing reduced DAF-2 pathway activity from the germline to the soma. Furthermore, results from our initial RNAi screen suggest dual roles of germline phosphoproteins in mediating the effects of IIS on reproduction and lifespan regulation. Notice that germline phosphoproteins are not necessarily germline-specific proteins. Techniques for tissue-specific mutagenesis of phosphosites are currently unavailable. Still, as a start, targeted protein degradation technologies, such as the AID method[43] used in the present study, are clearly helpful for testing hypotheses about tissue-specific signal transduction of IIS.

iFPS Together with Quantitative Phosphoproteomics as a General Approach to Study Functional Phosphorylation in vivo

We thoroughly mapped and quantified the IIS-regulated phosphorylation changes in *C. elegans*. Our phosphoproteomic workflow yielded the largest-to-date phosphoproteome dataset, almost doubling the size of previously available *C. elegans* database entries. Further, we designed and implemented a machine learning based tool – iFPS – for systematically ranking the likely functional importance of worm phosphosites. Such a tool was not previously available for the *C. elegans* research community. iFPS scores, together with the in vivo phosphosites identified here, constitute a major resource for studies of phosphorylation and insulin signal transduction.

iFPS scored 15,266 phosphosites in total. 50% of the true positive phosphosites were successfully recalled from the top 5% iFPS ranking, which is a ten-fold increase the propensity to hit a functional phosphosites from the overall background. Therefore, we considered a top 5% ranking as an initial cutoff for prioritizing the phosphosites regulated by *daf-2*. This prioritization strategy successfully guided our

follow-up experiments, which successfully demonstrated multiple mechanisms of lifespan regulation by IIS at the level of phosphorylation. Notably, we also tested two phosphosites that were among top 10–13%. Our findings that they were not obviously impactful for regulating the lifespan of WT or *daf-2* worms offers another form of validation for the utility of iFPS-based prioritization. Conventionally, these sites would almost certainly have been selected as candidates for functional studies. First, they are from translation initiation factor EIF-5 protein, which is in line with the hypothesis that translational repression contributes to lifespan extension. Second, they are close neighbors, and one of them is regulated by *daf-2*. It is thus clear that our new resources can help overcome the frequently encountered struggle with misleading “negative results” in attempts to validate findings from phosphoproteomic analyses.

Together with powerful prioritization tools and sophisticated validation experiments, phosphoproteome-scale functional elucidation of phosphosites sets a new benchmark for studies of longevity. The current iFPS scoring system is an encouraging start. The prediction power has not been fully explored owing to a paucity of experimentally confirmed functional phosphosites, kinase-substrate relations, protein-protein interactions, and other PTMs in *C. elegans*. Thus, additional experimental data, further computational resources, and innovative research strategies will still be needed to better comprehend which data signals actually convey informative hints to support identification of functional phosphosites in the future. Nevertheless, our study illustrates how our present strategy can be generally applied for a potentially wide range of other studies examining complicated biological phenomena to inform both basic mechanistic research and rational drug design.

Methods

C. elegans and *E. coli* strains

The genotypes, sources, and generating methods of *C. elegans* strains are listed in Supplementary Table 6. Worms were maintained on Nematode Growth Media (NGM) agar plates seeded with *E.coli* strain OP50 at 20 °C using standard protocols[62], unless otherwise indicated.

The ^{15}N-labeled food source was prepared by growing E. coli MG1655 in M9 minimal media ($^{15}NH_4Cl$ as the unique nitrogen source) until OD600 value reached to 1.0 at 37 °C[63]. MG1655 were concentrated and seeded on nitrogen-free worm plates.

E. coli HT115 transferred with RNAi plasmids or the empty vector control were cultured overnight in LB plus ampicillin (100 μg/ml) and tetracycline (10 μg/ml) and then seed on NGM plates containing ampicillin (100 μg/ml), tetracycline (10 μg/ml), and IPTG (1 mM). RNAi clones made in this paper were constructed by inserting the cDNA of genes into the L4440 vector. Other RNAi bacteria were derived from Ahringer RNAi library or RCE1181 *C. elegans* RNAi Feeding library.

Phosphoprotein sampling

Worms were synchronized by egg bleaching and overnight incubation in M9 buffer. The synchronized L1 larvae were fed with OP50 at 20ºC, harvested at adult day one, and subjected as unlabeled (^{14}N) *C. elegans* samples. The ^{15}N-labeled *C. elegans* reference sample was prepared by culturing N2 for generations on ^{15}N-labeled MG1655 at 20ºC and harvesting in mixed stages.

The ^{14}N and ^{15}N worms mixed at ratio 1:1 by volume were suspended in lysis buffer [2 × RIPA buffer, 2 × EDTA-free proteinase inhibitors cocktail (Roche), and 2 × PhosSTOP EASYpack (Roche)], homogenized in a FastPrep®-24 instrument (MP Biomedicals), and spun at 14,000 rpm for 30 min. The supernatants were precipitated and resolved in urea solution (8 M urea, 100 mM Tris-HCl, pH 8.5).10 mg total proteins determined by Bradford assay were subjected to reduction (5 mM TCEP), alkylation (10 mM Iodoacetamide), and trypsin digestion (overnight at 37 °C). The resulting products were fractionated on an Xtimate™ C18 reversed phase HPLC column (10 × 250 mm, 5 um, Welch Materials) using an Agilent 1200 Series HPLC instrument[19, 20]. Solvent A (2% acetonitrile, 10 mM ammonium formate, pH 10) and solvent B (90% acetonitrile, 10 mM ammonium formate, pH 10) were used to separate peptides at a flow rate of 3 ml/min. A nonlinear gradient was programmed with 5 different slopes (0% for 2 min; 0–10% in 5 min; 10–27% in 34 min; 27–31% in 4 min; 31–39% in 4 min; 39–60% in 7 min; 60% for 8 min). Eluted peptides were collected throughout the gradient with 0.66 min (= 2 ml) per fraction. The non-contiguous fractions were combined into 11 or 13 samples. After acidification and desalination, each fractionation was subjected to enrichment via PolyMAC-Ti enrichment kit (Tymora Analytical). The resulting phosphopeptides were resolved in 20 µl buffer (0.25% formic acid).

Mass spectrometry data acquisition

Samples was analyzed twice though a Q-Exactive mass spectrometer (Thermo Fisher Scientific) interfaced with an Easy-nLC1000 reversed-phase chromatography system (Thermo Fisher Scientific). 5 µl sample was loaded on a 75 µm × 4 cm trap column packed with 10 µm, 120 Å ODS-AQ C18 resin (YMC Co.) and separated by a 75 µm × 10 cm analytical column packed with 1.8 µm, 120 Å UHPLC XB-C18 resin (Welch Materials) at a flow rate of 200 nl/min using a linear gradient of 0–28% ACN (0.1% formic acid) over 80 min, followed by raising the ACN concentration to 80% within 15 min and maintaining for another 15 min.

The FTMS full scan between 350–2000 m/z were acquired from the Orbitrap at 70,000 resolution in profile data type with 1e6 AGC target, 60 ms maximum injection time. Ion 445.12003 was used for internal calibration. Top ten most abundant precursor ions were selected using a 2.0 m/z isolation window for HCD fragmentation (27% collision energy). MS2 scans were acquired from the Orbitrap at 17,500 resolution in profile data type with 5e4 AGC target, 250 ms maximum injection time. The intensity threshold for MS2 scan was 4e3. Precursors with + 1, > +6, and unassigned charge state were excluded. Peptide match was set as preferred. Dynamic exclusion was 60 s.

Phosphopeptide identification and phosphosite localization

Raw mass spectrometry files were searched against a composite target/decoy database using ProLuCID[64]. The *C. elegans* protein database (WS233) was used as target while the corresponding reversed sequences was generated as decoy. Spectra were searched with ± 50 ppm for both precursor ion and fragment ion accuracy, peptide length above 7 residues, fully tryptic restriction. Carbamidomethylation of cysteines was included as a fixed modification. Phosphorylation of serine, threonine and tyrosine residues were included as variable modifications. The peptide spectrum matches were filtered using DTASelect2 [65]. The estimated false discovery rate (FDR) was no more than 1.07% for phosphopeptides. The ^{14}N and ^{15}N-labeled peptides were identified in paralleled pipelines.

For each ^{14}N peptide, phosphosites with phosphoRS site probability[23] above 0.75 were assigned as confident modification. The phosphosite localization on the ^{15}N-labeled peptide was corrected corresponding to its ^{14}N-isotopic version. The residual number of phosphosites was determined by mapping the phosphopeptides to the longest transcripts of *C. elegans* genes (UniProt 201501). Phosphosites from single-phosphorylated peptides and multi-phosphorylated peptides were extracted as different phosphoisoforms (see examples in Supplementary Fig. 1C).

Phosphoisoform quantification

Ratios of ^{14}N to ^{15}N-labeled phosphopeptide were determined by a modified version of pQuant software[66]. In brief, confident quantification was accepted when both the least interfered isotopic ratio and the monoisotopic ratio of a ^{14}N and ^{15}N ion pair had the σ values below 0.5. The median of least interfered ratios was assigned as the $^{14}N/^{15}N$ ratios of quantified peptides. Ratios were normalized to the median value of all quantified peptides per technical replicates, and then assigned to their corresponding phosphoisoforms.

Phosphorylation changes in IIS mutants

To determine the *daf-2* regulated phosphorylation, phosphoisoforms, which were quantified at least three times in both *daf-2* and WT, were subjected to statistical comparison. We noticed that 1125 phosphoisoforms, which were reliably measured more than twice in *daf-2* samples were only quantified once or twice in WT samples. In this scenario, if the quantitation values in *daf-16* and/or *daf-16; daf-2* samples were similar to those in WT, we manually imputed the values quantified in the WT-like short-lived controls to the WT samples. Log2 (median of *daf-2/* median of control) distribution was plotted to estimate the median and s.iqr values. The $^{14}N/^{15}N$ ratios of each phosphoisoforms were subjected to Wilcoxon rank-sum test. A “strict” filter was applied with log2 (*daf-2/*control) fold change above a factor 1.5 (s.iqr, in either direction) and $p < 0.05$ from the Wilcoxon rank-sum test. A “loose” subset of *daf-2* regulated phosphoisoforms met the criteria of either (log2 (*daf-2/*control) changed above a factor 1.5 while $p \leq 0.1$) or (log2 (*daf-2/*WT) changed at least a factor 1 while $p < 0.05$).

Similarly, phosphoisoforms quantified at least three times in both *daf-2* and *daf-16; daf-2*, were subjected to statistical comparison. Phosphorylation changed in *daf-16; daf-2* comparing to *daf-2* was determined

by a “loose” filter (log2 (*daf-2/daf-16; daf-2*) beyond 1.5 s.iqr and $p \leq 0.10$ or log2 (*daf-2/daf-16; daf-2*) beyond 1.0 s.iqr and $p < 0.05$, Wilcoxon rank-sum test). The *daf-2* regulated phosphoisoforms whose phosphorylation changed in *daf-16; daf-2* vs *daf-2* were determined as *daf-16*-dependent phosphoisoforms. The *daf-2* regulated phosphoisoforms whose phosphorylation remained similar in *daf-16; daf-2* vs *daf-2* were determined as *daf-16*-independent phosphoisoforms.

Prioritization of the potentially important phosphosites

iFPS (Inference of Functional Phosphorylation Sites) algorithm was developed to systematically rank the functional importance of *C. elegans* phosphosites. Constraints that may indicate the biological impacts of phosphosites were selected based on a survey of literature. The following six constraints were estimated on their potential to discriminate functional phosphosites in *C. elegans*, and were further integrated into one score by a machine learning method.

1. Kinase families

Functional phosphosites are often regulated by kinases. A previous developed software package iGPS 1.0[45] was used to predict kinases that recognize individual phosphosite. For a better coverage, low thresholds with false positive rates (FDRs) of 10% for serine/threonine kinases and 15% for tyrosine kinases were adopted. Potentially false-positive hits were filtered by using protein-protein interaction information integrated in iGPS. Numbers of kinase families targeting each phosphosite were evaluated and selected as a predictor of functional phosphorylation.

2. Conservation

Comparing to sequence conservation, phosphorylation conservation is a better predictor of functional phosphosites. Phosphorylation conservation was indicated by RCS value as described below.

Sequences of the *C. elegans* phosphoproteins were multi-aligned by MUSCLE[67] to their orthologs which were pairwisely detected by iterative BLAST[68] in other six eukaryotes (*H. sapiens*, *M. musculus*, *R. norvegicus*, *D. melanogaster*, *S. cerevisiae*, and *S. pombe)*. The conservation of phosphorylated and non-phosphorylated serine, threonine, and tyrosine (S/T/Y) residues were indicated by Residue Conservation Score (RCS)[69].

RCS = MBL × RCR

The Maximum Branch Length (MBL) is the longest evolutionary distance between any two organisms that containing a conserved pS/pT/pY or S/T/Y. A phylogenetic tree built by Interactive Tree Of Life (iTOL, https://itol.embl.de/)[70] was used for estimating evolutionary distance. The Residue Conservation Ratio (RCR) is defined as percentage of conserved residue at desired position across the organisms that are within the MBL.

3. Protein-protein interactions (PPI) domain

Phosphosites at the interacting domains are potential regulators of PPI. Based on Pfam 31.0 database[71], domain families of all phosphoproteins were predicted using the hmmsearch program in the HMMER v3.1b2 package[72]. The domain-domain and domain-motif interactions were derived from 3DID database[73]. The phosphosite resided domains and motifs that participate in PPI were counted.

4. Crosstalk

Adjacent PTMs may co-regulate a biological event, for example histone acetylation and phosphorylation are synergistic in remodeling chromatin structure of target genes. GPS-PAIL 2.0, a software developed to predict the histone acetyltransferases (HATs)-specific sites[74] was applied to predict acetylation sites close to phosphosites. The *C.elegans* orthologs of five HATs (EP300, HAT1, KAT2B, KAT5 and KAT8) were considered as potential regulators. For a better coverage, low thresholds with specificity (Sp) values of 85% was adopted. The phosphosite with at least one acetylation site located within 15 amino acids was assigned with a crosstalk value of 1, otherwise the value was 0.

5. Relative surface accessibility (RSA) and secondary structure

The accessibility and structure environment around phosphosites affect their chance to be targeted by specific kinases. Here, the surface accessibility and secondary structure of phosphosites were predicted by the webserver of NetSurfP v1.1 (http://www.cbs.dtu.dk/services/NetSurfP/)[75]. The RSA scores and the probabilities for Alpha-Helix, Beta-strand and Coil of each phosphosite were used for model training and prediction.

For model training, the manually compiled 121 known functional phosphosites of *C. elegans* were used as positive data set (Supplementary Table 2). Other *C.elegans* phosphosites in dbPAF database were selected as negative samples. The multinomial logistic regression model with a ridge estimator in Java package Weka 3.8[76] was adopted for training. Due to the much larger size of negative samples, the performance and robustness of prediction system were evaluated with different ratios (1:1, 1:2, 1:5 and 1:10) of positive and negative samples. Ratio of 1:5 won best. Therefore, 10 sets of 5 times negative samples were randomly selected for the training. The model with the best performance was chosen as the final model. 10-fold cross validate model was used to avoid overfitting during training.

Target quantification of phosphorylation and proteins

Endogenous levels of target phosphorylation and protein were quantified by LC-MS/MS analysis of the worm proteome using isotopically labeled peptides as a spike-in standard. Total proteins were extracted from adult day one worms by cryogenic grinding (mixer mill MM 400, Retsch) and resolved in lysis buffer (0.1 M Tris/HCl, pH 7.6, 4% SDS, 0.1 M DTT, protease inhibitor cocktail, and phosphatase inhibitor cocktail). The crude extract was incubated at 95 °C for 5 min followed by centrifugation at 14,000 rpm (10 min, room temperature). Supernatant was collected and sent for protein concentration measurement by 2-D quant. 100 µg of total proteins were subjected to buffer exchange, alkylation reaction and trypsin

digestion by the filter-aided sample preparation (FASP) method[77]. The synthesized isotopically labeled peptides were simultaneously spiked in right before adding trypsin (see Supplementary Table 5).

After 18 hours digestion, the peptide mixture was centrifuged at 14,000 rpm (30 min, 4 °C). Each sample with 5–10 μg peptides were analyzed twice on a Q-Exactive mass spectrometer (Thermo Fisher Scientific) interfaced with an Easy-nLCII liquid chromatography system (Thermo Fisher Scientific). Homemade 75 μm × 4 cm trap columns (ReproSil-Pur 120 C18-AQ, 3 μm, Dr. Maisch GmbH) and 75 μm × 12 cm analytical columns (ReproSil-Pur 120 C18-AQ, 1.9 μm, Dr. Maisch GmbH) were heated to 60 °C for online desalting followed by separation at a flow rate of 200 nl/min with a linear gradient (0% B at 0 min, 12% B at 1 min, 25% B at 61 min, 80% B at 71 min, 80% B at 81 min). Solvent A and B were 0.1% (v/v) FA in water and 0.1% (v/v) FA in acetonitrile, respectively.

Peptides were mobilized in the positive-ion mode by electrospray ionization with 2 kV spray voltage and 320 °C capillary temperature. Ion 445.120025 m/z was used for internal calibration. Full-scan mass spectra were acquired in the Orbitrap over the m/z range of 300 to 1500 at a resolution of 70,000. AGC target was set to 3e6. Maximum injection time was 60 ms. Precursor ions of target peptides were selected for Higher-energy Collisional Dissociation (HCD) fragmentation and Orbitrap detection during desired acquisition time. The operating parameters were: resolution 35,000; AGC targets 1e5; maximum IT auto; isolation window 2 m/z; normalized collision energy 27.

MS data were processed in Xcalibur (version 2.2 SP1.48, Thermo Fisher Scientific) and pLabel (version 2.4)[78]. Isotopically labeled peptide ions were used to locate the endogenous targets across the elution. For each target precursor ion, at least three fragment ions with high abundance and low interference were selected for identification and quantitation. Peaks areas of precursor ions generating each desired fragment ion were determined in Xcalibur with default parameter and used for quantification.

Endogenous peptides (light ions) and their isotopically labeled counterparts (heavy ions) were quantified by extracting peak areas of each quantifiable transition (precursor → fragment). For each transition, peak areas of light were divided by that of heavy. Relative abundance of individual phosphorylation or protein was determined by the mean value of light/heavy ratios. Two-tailed p value comparing quantitation in IIS mutants to WT was calculated by Student's *t* test.

CRISPR/Cas9 based mutagenesis

The CRISPR/Cas9-mediated mutagenesis of *C. elegans* endogenous genes was performed as described with little modification[79, 80, 81]. For the sgRNA-Cas9 expression plasmid-based mutagenesis, individual sgRNA was incorporated into the pDD162 plasmid (Addgene, #47549) at desired locus. Usually two different sgRNAs were used simultaneously. For the Cas9 ribonucleoprotein-based mutagenesis, a crRNA that contains the target sequence at the 5' end was synthesized. Two or more alleles relating to each target were assayed in follow-up studies.

To specifically deplete WEE-1.3 in the germline of *C. elegans*, reagents for the auxin-induced degradation (AID) system were developed as previously reported[43]. The *mNeonGreen::degron* cassette was inserted adjacent to the ATG codon of endogenous *wee-1.3* by the CRIPSR/Cas9 technology. Three different sgRNA-Cas9 vectors and one template plasmid together with injection markers were co-injected into young adults of CA1199 *(unc-119(ed3) III; ieSi38[sun-1p::TIR1::mRuby::sun-1 3'UTR + Cbr-unc-119(+)] IV)* strain.

Western blot analysis

Synchronized worms of each strain were grown on OP50 plates at 20 °C and harvested at adult day one using M9 buffer, followed by liquid nitration freezing. Worm pellets were boiled in SDS loading buffer and loaded to replicate SDS-PAGE gels. The transferred fluorescence PVDF membranes (Millipore) were probed overnight at 4 °C with anti-phospho-eIF2α (Ser51) and anti-eIF2α (kindly provided by Dr. Shin Takagi) primary antibody, respectively. The blots were visualized by one-hour incubation at room temperature with IRDye 800CW fluorescent secondary antibodies (Odyssey), followed by scanning in the LI-COR Odyssey Infrared Imaging System according to the manufacturer's instruction. Images were quantified with Image Studio Lite Ver 4.0 (LI-COR). The significance of intensity difference was evaluated by paired *t* test. To examine the AKT-1::GFP level, nitrocellulose membranes were probed with anti-GFP or anti-tubulin antibodies. HRP conjugated secondary antibodies were used for detection.

Lifespan assays

Lifespan assays were modified based on previous description[15]. Worms were synchronized via collecting eggs laid within 4 hours by adult day two hermaphrodites. Worms were transferred to desired plates (25 to 35 worms per plate) when they reached adulthood, and continually transferred to fresh plates every other day. After they ceased laying egg, living worms were scored every two days and transferred to fresh plates every four to seven days. Statistical analysis of lifespan data was performed in SPSS software. Replicates as well as measuring conditions including temperature and supplements in plates are recorded in Supplementary Table 4.

Auxin treatment was performed as previous description[43]. Briefly, auxin, which was dissolved in ethanol was added to NGM agar before pouring plates. The final concentration of auxin and ethanol per plate was 1 mM and 0.25%, respectively. 0.25% ethanol was used as control.

For TBB treatment, TBB was resolved in 80% DMSO: PBS solvent. NGM plates containing 50 ng/μl FUDR were seeded with OP50 and dried at room temperature for 12 hours. Then TBB solution was added to the surface of plates with the final concentration of 15 uM or 45 uM TBB. The final concentration of DMSO for each plate was adjusted to 0.36%, including the control. Supplied volume is based on the volume of media. The freshly prepared plates were left for drug diffusion overnight and used within two days. Synchronized adult day one WT were transferred to plates with TBB or control treatment at 20 °C. After 24 or 48 hours, worms were moved to fresh NGM plates (50 ng/μl FUDR).

Dauer formation

Parent worms were maintained on NGM plates seeded with OP50 at 15 °C for over three generations and allowed to lay eggs for 4–6 hours at 21 °C. Progeny were incubated at 21 °C. Dauer and non-dauer animals were scored and confirmed at the third, fourth, or fifth day post egg-laying.

Polyribosome profiling assays

Polyribosome profiling was performed as previous description with little modification[9]. 10 ml 7–50% (w/v) linear sucrose gradients in gradient buffer (110 mM KAc, 20 mM MgAc2 and 10 mM HEPES pH 7.6) were prepared in 13 ml polyallomer centrifuge tubes (Beckman-Coulter) just before use. Adult day one synchronized worms were lysed in lysis buffer (30 mM HEPES pH 7.6, 100 mM KCl, 10 mM $MgCl_2$, 0.1% NP-40, 100 mg/ml cycloheximide, 2 mM DTT, 40 U/ml RNase inhibitor, and protease inhibitor cocktail) with a dounce homogenizer. Worm lysate was centrifuged at 14,000 g (10 min, 4 °C). The supernatant was immediately subject to protein content estimation by $A_{280\ nm}$ on NanoDrop 1000 (Thermo Fisher Scientific). The same amount of $A_{280\ nm}$ units (3000–6100 units) of each sample was layered atop the 7–50% (w/v) linear sucrose gradient and centrifuged for two hours at 40,000 rpm in a SW41Ti rotor (Beckman-Coulter) at 4 °C. Gradients were analyzed with a density gradient fractionator coupled with the absorbance recording at an optical density of 254 nm (Teledyne Isco). Images were transferred into digital data using Adobe Photoshop and merged by aligning base line of absorbance using Adobe Illustrator.

Microscopy

Worms were cultured at 20 °C. To measure the cellular localization of DAF-16::GFP, L4 or young adult worms were picked on pad and visualized under fluorescent microscopy within two minutes. DAF-16::GFP localization in intestinal cells was manually classified (Fig. 3C). The number of worms in each category was counted. Images were taken using a Zeiss Axio Imager M1 microscope at 400-fold magnification. Images of worms expressing AKT-1::GFP or AKT-T492A::GFP were taken by the Zeiss Axio Imager M1 microscope at 100-fold or 200-fold magnification. The penetrance of AKT-1-T492A::GFP nuclear localization in proximal gonad was calculated by scoring the number of worms under the same microscope at 1000-fold magnification. Fluorescence images of AKT-1::GFP or AKT-T492A::GFP in the germline were acquired using a Spinning Disk microscope.

Tissue expression prediction

Proteins with decreased or increased phosphorylation on the *daf-2* regulated phosphoisoform were defined as hypo- or hyper-phosphorylated proteins respectively. 180 hypo- and 169 hyper-phosphorylated proteins were mapped, 8 of which were shared by both. Expression of the *daf-2* regulated phosphoproteins across 76 tissues and cell types were implemented on an interactive webserver (http://worm.princeton.edu)[82]. The prediction scores were downloaded for statistical enrichment calculation using R software (v.3.5.0). The two-tailed p value per sub-tissue was calculated by Z-test.

Kinase substrate analysis

The iGPS-predicted kinase-substrate relations were adopted for kinase substrate analysis. Hypergeometric test followed by Benjamini-Hochberg adjustment was used to determine whether targets of particular kinases were enriched in the *daf-2* hyper-or hypo-phosphorylated dataset by setting all *C. elegans* phosphosites as background. Alternatively, Motif-X (http://motif-x.med.harvard.edu/motif-x.html) was performed to identify the significantly overrepresented motifs, with the default parameters (width = 13, occurrences = 20, and significance < 1E-6) and the total quantified phosphopeptides as background.

Data And Code Availability

The MS raw data for phosphoproteomics and target quantitation in this study are deposited to the ProteomeXchange Consortium via the iProX partner repository[83] with the dataset identifier PXD020440 (https://www.iprox.org/page/PSV023.html;?url=1595231837574FhIp, password “yXtx”). Code and functions used to generate iFPS are available online (https://github.com/CuckooWang/iFPS).

Declarations

Competing Interests

The authors declare no competing interests.

Author Contributions

Conception, W.J.L., C.W.W., Y.X., and M.Q.D.; Design of the work, W.J.L., L.T., C.W.W., Y.X., and M.Q.D.; Analysis, W.J.L., L.T., C.W.W., Y.H.Y., M.J.Z., Y.X.L., Z.X.L., and H.Q.Z.; Acquisition, W.J.L., L.T., Y.H.Y., X.M.L., and X.D.H.; Writing, W.J.L., C.W.W., Y.X., and M.Q.D.; Visualization, W.J.L. and C.W.W.; Supervision, Y.X. and M.Q.D.; Funding Acquisition, Y.X. and M.Q.D.

Acknowledgments

We are grateful to Drs. Yan-Ping Zhang and Wen-Hong Zhang for constructing and sharing the *daf-16(hqKi23)* and *daf-2(hqKi363)* strains. We thank Dr. Shin Takagi for the EIF-2α antibody, Dr. Di Chen for the *rrf-1(pk1417)* strain, and members of M.Q.D.’s lab for scientific discussion. We also thank the Caenorhabditis Genetics Center (CGC) and WormBase for managing and providing worm resources. CGC is supported by the NIH Office of Research Infrastructure Programs (P40 OD010440). WormBase is supported by grant #U24 HG002223 from the National Human Genome Research Institute at the US National Institutes of Health, the UK Medical Research Council and the UK Biotechnology and Biological Sciences Research Council. This research was funded by Ministry of Science and Technology of China

(2014CB84980001 to M.-Q.D.), Beijing Municipal Science and Technology Commission, Special Project on Precision Medicine under the National Key R&D Program (2018YFC0910500 to Y.X.), the Natural Science Foundation of China (31930021, 31970633, 31671360, and 81701567 to Y.X.), the Fundamental Research Funds for the Central Universities (2017KFXKJC001 and 2019kfyRCPY043 to Y.X.), Changjiang Scholars Program of China, and the program for HUST Academic Frontier Youth Team.

References

1. Kenyon CJ. The genetics of ageing. *Nature* 2010, **464**(7288): 504–512.
2. Singh PP, Demmitt BA, Nath RD, Brunet A. The Genetics of Aging: A Vertebrate Perspective. *Cell* 2019, **177**(1): 200–220.
3. Ayyadevara S, Alla R, Thaden JJ, Shmookler Reis RJ. Remarkable longevity and stress resistance of nematode PI3K-null mutants. *Aging cell* 2008, **7**(1): 13–22.
4. Murphy CT, Hu PJ. Insulin/insulin-like growth factor signaling in C. elegans. *WormBook: the online review of C elegans biology* 2013: 1–43.
5. Narayan V, Ly T, Pourkarimi E, Murillo AB, Gartner A, Lamond AI, *et al.* Deep Proteome Analysis Identifies Age-Related Processes in C. elegans. *Cell systems* 2016, **3**(2): 144–159.
6. Walther DM, Kasturi P, Zheng M, Pinkert S, Vecchi G, Ciryam P, *et al.* Widespread Proteome Remodeling and Aggregation in Aging C. elegans. *Cell* 2015, **161**(4): 919–932.
7. Depuydt G, Xie F, Petyuk VA, Shanmugam N, Smolders A, Dhondt I, *et al.* Reduced insulin/insulin-like growth factor-1 signaling and dietary restriction inhibit translation but preserve muscle mass in Caenorhabditis elegans. *Molecular & cellular proteomics: MCP* 2013, **12**(12): 3624–3639.
8. Depuydt G, Xie F, Petyuk VA, Smolders A, Brewer HM, Camp DG, 2nd, *et al.* LC-MS proteomics analysis of the insulin/IGF-1-deficient Caenorhabditis elegans daf-2(e1370) mutant reveals extensive restructuring of intermediary metabolism. *Journal of proteome research* 2014, **13**(4): 1938–1956.
9. Stout GJ, Stigter EC, Essers PB, Mulder KW, Kolkman A, Snijders DS, *et al.* Insulin/IGF-1-mediated longevity is marked by reduced protein metabolism. *Molecular systems biology* 2013, **9**: 679.
10. Padmanabhan S, Mukhopadhyay A, Narasimhan SD, Tesz G, Czech MP, Tissenbaum HA. A PP2A regulatory subunit regulates C. elegans insulin/IGF-1 signaling by modulating AKT-1 phosphorylation. *Cell* 2009, **136**(5): 939–951.
11. Sen I, Zhou X, Chernobrovkin A, Puerta-Cavanzo N, Kanno T, Salignon J, *et al.* DAF-16/FOXO requires Protein Phosphatase 4 to initiate transcription of stress resistance and longevity promoting genes. *Nature communications* 2020, **11**(1): 138.
12. Chen YC, Chen HJ, Tseng WC, Hsu JM, Huang TT, Chen CH, *et al.* A C. elegans Thermosensory Circuit Regulates Longevity through crh-1/CREB-Dependent flp-6 Neuropeptide Signaling. *Developmental cell* 2016, **39**(2): 209–223.
13. Lin K, Hsin H, Libina N, Kenyon C. Regulation of the Caenorhabditis elegans longevity protein DAF-16 by insulin/IGF-1 and germline signaling. *Nature genetics* 2001, **28**(2): 139–145.

14. Mair W, Morantte I, Rodrigues AP, Manning G, Montminy M, Shaw RJ, *et al.* Lifespan extension induced by AMPK and calcineurin is mediated by CRTC-1 and CREB. *Nature* 2011, **470**(7334): 404–408.
15. Tao L, Xie Q, Ding YH, Li ST, Peng S, Zhang YP, *et al.* CAMKII and calcineurin regulate the lifespan of Caenorhabditis elegans through the FOXO transcription factor DAF-16. *eLife* 2013, **2**: e00518.
16. Zhang Y, Lanjuin A, Chowdhury SR, Mistry M, Silva-Garcia CG, Weir HJ, *et al.* Neuronal TORC1 modulates longevity via AMPK and cell nonautonomous regulation of mitochondrial dynamics in C. elegans. *eLife* 2019, **8**.
17. Ullah S, Lin S, Xu Y, Deng W, Ma L, Zhang Y, *et al.* dbPAF: an integrative database of protein phosphorylation in animals and fungi. *Scientific reports* 2016, **6**: 23534.
18. Ochoa D, Jarnuczak AF, Vieitez C, Gehre M, Soucheray M, Mateus A, *et al.* The functional landscape of the human phosphoproteome. *Nature biotechnology* 2020, **38**(3): 365–373.
19. Batth TS, Francavilla C, Olsen JV. Off-line high-pH reversed-phase fractionation for in-depth phosphoproteomics. *Journal of proteome research* 2014, **13**(12): 6176–6186.
20. Yang F, Shen Y, Camp DG, 2nd, Smith RD. High-pH reversed-phase chromatography with fraction concatenation for 2D proteomic analysis. *Expert review of proteomics* 2012, **9**(2): 129–134.
21. Iliuk A, Jayasundera K, Wang WH, Schluttenhofer R, Geahlen RL, Tao WA. In-Depth Analyses of B Cell Signaling Through Tandem Mass Spectrometry of Phosphopeptides Enriched by PolyMAC. *International journal of mass spectrometry* 2015, **377**: 744–753.
22. Iliuk AB, Martin VA, Alicie BM, Geahlen RL, Tao WA. In-depth analyses of kinase-dependent tyrosine phosphoproteomes based on metal ion-functionalized soluble nanopolymers. *Molecular & cellular proteomics: MCP* 2010, **9**(10): 2162–2172.
23. Taus T, Kocher T, Pichler P, Paschke C, Schmidt A, Henrich C, *et al.* Universal and confident phosphorylation site localization using phosphoRS. *Journal of proteome research* 2011, **10**(12): 5354–5362.
24. Kimura KD, Tissenbaum HA, Liu Y, Ruvkun G. daf-2, an insulin receptor-like gene that regulates longevity and diapause in Caenorhabditis elegans. *Science* 1997, **277**(5328): 942–946.
25. McElwee JJ, Schuster E, Blanc E, Thornton J, Gems D. Diapause-associated metabolic traits reiterated in long-lived daf-2 mutants in the nematode Caenorhabditis elegans. *Mechanisms of ageing and development* 2006, **127**(5): 458–472.
26. Zhang P, Judy M, Lee SJ, Kenyon C. Direct and indirect gene regulation by a life-extending FOXO protein in C. elegans: roles for GATA factors and lipid gene regulators. *Cell metabolism* 2013, **17**(1): 85–100.
27. Beltrao P, Albanese V, Kenner LR, Swaney DL, Burlingame A, Villen J, *et al.* Systematic functional prioritization of protein posttranslational modifications. *Cell* 2012, **150**(2): 413–425.
28. Needham EJ, Parker BL, Burykin T, James DE, Humphrey SJ. Illuminating the dark phosphoproteome. *Science signaling* 2019, **12**(565).

29. Facchinetti V, Ouyang W, Wei H, Soto N, Lazorchak A, Gould C, *et al.* The mammalian target of rapamycin complex 2 controls folding and stability of Akt and protein kinase C. *The EMBO journal* 2008, **27**(14): 1932–1943.
30. Oh WJ, Wu CC, Kim SJ, Facchinetti V, Julien LA, Finlan M, *et al.* mTORC2 can associate with ribosomes to promote cotranslational phosphorylation and stability of nascent Akt polypeptide. *The EMBO journal* 2010, **29**(23): 3939–3951.
31. Zhang Y, Xu J, Puscau C, Kim Y, Wang X, Alam H, *et al.* Caenorhabditis elegans EAK-3 inhibits dauer arrest via nonautonomous regulation of nuclear DAF-16/FoxO activity. *Developmental biology* 2008, **315**(2): 290–302.
32. Schuster E, McElwee JJ, Tullet JM, Doonan R, Matthijssens F, Reece-Hoyes JS, *et al.* DamID in C. elegans reveals longevity-associated targets of DAF-16/FoxO. *Molecular systems biology* 2010, **6**: 399.
33. Son HG, Seo M, Ham S, Hwang W, Lee D, An SW, *et al.* RNA surveillance via nonsense-mediated mRNA decay is crucial for longevity in daf-2/insulin/IGF-1 mutant C. elegans. *Nature communications* 2017, **8**: 14749.
34. Filer D, Thompson MA, Takhaveev V, Dobson AJ, Kotronaki I, Green JWM, *et al.* RNA polymerase III limits longevity downstream of TORC1. *Nature* 2017, **552**(7684): 263–267.
35. Hansen M, Taubert S, Crawford D, Libina N, Lee SJ, Kenyon C. Lifespan extension by conditions that inhibit translation in Caenorhabditis elegans. *Aging cell* 2007, **6**(1): 95–110.
36. Pan KZ, Palter JE, Rogers AN, Olsen A, Chen D, Lithgow GJ, *et al.* Inhibition of mRNA translation extends lifespan in Caenorhabditis elegans. *Aging cell* 2007, **6**(1): 111–119.
37. Nukazuka A, Fujisawa H, Inada T, Oda Y, Takagi S. Semaphorin controls epidermal morphogenesis by stimulating mRNA translation via eIF2alpha in Caenorhabditis elegans. *Genes & development* 2008, **22**(8): 1025–1036.
38. Sonenberg N, Hinnebusch AG. Regulation of translation initiation in eukaryotes: mechanisms and biological targets. *Cell* 2009, **136**(4): 731–745.
39. Boxem M, Srinivasan DG, van den Heuvel S. The Caenorhabditis elegans gene ncc-1 encodes a cdc2-related kinase required for M phase in meiotic and mitotic cell divisions, but not for S phase. *Development* 1999, **126**(10): 2227–2239.
40. Boxem M. Cyclin-dependent kinases in C. elegans. *Cell division* 2006, **1**: 6.
41. Michaelson D, Korta DZ, Capua Y, Hubbard EJ. Insulin signaling promotes germline proliferation in C. elegans. *Development* 2010, **137**(4): 671–680.
42. Kumsta C, Hansen M. C. elegans rrf-1 mutations maintain RNAi efficiency in the soma in addition to the germline. *PloS one* 2012, **7**(5): e35428.
43. Zhang L, Ward JD, Cheng Z, Dernburg AF. The auxin-inducible degradation (AID) system enables versatile conditional protein depletion in C. elegans. *Development* 2015, **142**(24): 4374–4384.

44. Hsin H, Kenyon C. Signals from the reproductive system regulate the lifespan of C. elegans. *Nature* 1999, **399**(6734): 362–366.
45. Song C, Ye M, Liu Z, Cheng H, Jiang X, Han G, *et al.* Systematic analysis of protein phosphorylation networks from phosphoproteomic data. *Molecular & cellular proteomics: MCP* 2012, **11**(10): 1070–1083.
46. Chou MF, Schwartz D. Biological sequence motif discovery using motif-x. *Current protocols in bioinformatics* 2011, Chap. 1**3**: Unit 13 15–24.
47. Park JH, Lee JH, Park JW, Kim DY, Hahm JH, Nam HG, *et al.* Downregulation of protein kinase CK2 activity induces age-related biomarkers in C. elegans. *Oncotarget* 2017, **8**(23): 36950–36963.
48. Kang WK, Kim YH, Kang HA, Kwon KS, Kim JY. Sir2 phosphorylation through cAMP-PKA and CK2 signaling inhibits the lifespan extension activity of Sir2 in yeast. *eLife* 2015, **4**.
49. Fabrizio P, Hoon S, Shamalnasab M, Galbani A, Wei M, Giaever G, *et al.* Genome-wide screen in Saccharomyces cerevisiae identifies vacuolar protein sorting, autophagy, biosynthetic, and tRNA methylation genes involved in life span regulation. *PLoS genetics* 2010, **6**(7): e1001024.
50. Williams GC. Pleiotropy, natural selection, and the evolution of senescence. *Evolution* 1957, **11**: 398–411.
51. Essers PB, Nonnekens J, Goos YJ, Betist MC, Viester MD, Mossink B, *et al.* A Long Noncoding RNA on the Ribosome Is Required for Lifespan Extension. *Cell reports* 2015, **10**(3): 339–345.
52. Rousakis A, Vlassis A, Vlanti A, Patera S, Thireos G, Syntichaki P. The general control nonderepressible-2 kinase mediates stress response and longevity induced by target of rapamycin inactivation in Caenorhabditis elegans. *Aging cell* 2013, **12**(5): 742–751.
53. D'Aniello C, Fico A, Casalino L, Guardiola O, Di Napoli G, Cermola F, *et al.* A novel autoregulatory loop between the Gcn2-Atf4 pathway and l-Proline metabolism controls stem cell identity. *Cell death and differentiation* 2015, **22**(7): 1234.
54. Ye J, Kumanova M, Hart LS, Sloane K, Zhang H, De Panis DN, *et al.* The GCN2-ATF4 pathway is critical for tumour cell survival and proliferation in response to nutrient deprivation. *The EMBO journal* 2010, **29**(12): 2082–2096.
55. Henis-Korenblit S, Zhang P, Hansen M, McCormick M, Lee SJ, Cary M, *et al.* Insulin/IGF-1 signaling mutants reprogram ER stress response regulators to promote longevity. *Proceedings of the National Academy of Sciences of the United States of America* 2010, **107**(21): 9730–9735.
56. Darnell AM, Subramaniam AR, O'Shea EK. Translational Control through Differential Ribosome Pausing during Amino Acid Limitation in Mammalian Cells. *Molecular cell* 2018, **71**(2): 229–243 e211.
57. Dong J, Qiu H, Garcia-Barrio M, Anderson J, Hinnebusch AG. Uncharged tRNA activates GCN2 by displacing the protein kinase moiety from a bipartite tRNA-binding domain. *Molecular cell* 2000, **6**(2): 269–279.
58. Gao AW, Smith RL, van Weeghel M, Kamble R, Janssens GE, Houtkooper RH. Identification of key pathways and metabolic fingerprints of longevity in C. elegans. *Experimental gerontology* 2018, **113**:

128–140.

59. Apfeld J, Kenyon C. Cell nonautonomy of C. elegans daf-2 function in the regulation of diapause and life span. *Cell* 1998, **95**(2): 199–210.
60. Libina N, Berman JR, Kenyon C. Tissue-specific activities of C. elegans DAF-16 in the regulation of lifespan. *Cell* 2003, **115**(4): 489–502.
61. Moll L, Roitenberg N, Bejerano-Sagie M, Boocholez H, Carvalhal Marques F, Volovik Y, *et al.* The insulin/IGF signaling cascade modulates SUMOylation to regulate aging and proteostasis in Caenorhabditis elegans. *eLife* 2018, **7**.
62. Brenner S. The genetics of Caenorhabditis elegans. *Genetics* 1974, **77**(1): 71–94.
63. Khan Z, Amini S, Bloom JS, Ruse C, Caudy AA, Kruglyak L, *et al.* Accurate proteome-wide protein quantification from high-resolution 15N mass spectra. *Genome biology* 2011, **12**(12): R122.
64. Xu T, Park SK, Venable JD, Wohlschlegel JA, Diedrich JK, Cociorva D, *et al.* ProLuCID: An improved SEQUEST-like algorithm with enhanced sensitivity and specificity. *Journal of proteomics* 2015, **129**: 16–24.
65. Cociorva D, D LT, Yates JR. Validation of tandem mass spectrometry database search results using DTASelect. *Current protocols in bioinformatics* 2007, Chap. 1**3**: Unit 13 14.
66. Liu C, Song CQ, Yuan ZF, Fu Y, Chi H, Wang LH, *et al.* pQuant improves quantitation by keeping out interfering signals and evaluating the accuracy of calculated ratios. *Analytical chemistry* 2014, **86**(11): 5286–5294.
67. Edgar RC. MUSCLE: multiple sequence alignment with high accuracy and high throughput. *Nucleic acids research* 2004, **32**(5): 1792–1797.
68. Tatusov RL, Koonin EV, Lipman DJ. A genomic perspective on protein families. *Science* 1997, **278**(5338): 631–637.
69. Minguez P, Parca L, Diella F, Mende DR, Kumar R, Helmer-Citterich M, *et al.* Deciphering a global network of functionally associated post-translational modifications. *Molecular systems biology* 2012, **8**: 599.
70. Letunic I, Bork P. Interactive tree of life (iTOL) v3: an online tool for the display and annotation of phylogenetic and other trees. *Nucleic acids research* 2016, **44**(W1): W242-245.
71. El-Gebali S, Mistry J, Bateman A, Eddy SR, Luciani A, Potter SC, *et al.* The Pfam protein families database in 2019. *Nucleic acids research* 2019, **47**(D1): D427-D432.
72. Potter SC, Luciani A, Eddy SR, Park Y, Lopez R, Finn RD. HMMER web server: 2018 update. *Nucleic acids research* 2018, **46**(W1): W200-W204.
73. Mosca R, Ceol A, Stein A, Olivella R, Aloy P. 3did: a catalog of domain-based interactions of known three-dimensional structure. *Nucleic acids research* 2014, **42**(Database issue): D374-379.
74. Deng W, Wang C, Zhang Y, Xu Y, Zhang S, Liu Z, *et al.* GPS-PAIL: prediction of lysine acetyltransferase-specific modification sites from protein sequences. *Scientific reports* 2016, **6**: 39787.

75. Petersen B, Petersen TN, Andersen P, Nielsen M, Lundegaard C. A generic method for assignment of reliability scores applied to solvent accessibility predictions. *BMC structural biology* 2009, **9**: 51.
76. Hall M, Frank E, Holmes G, Pfahringer B, Reutemann P, Witten IH. The WEKA data mining software: an update. *ACM SIGKDD explorations newsletter* 2009, **11**(1): 10–18.
77. Wisniewski JR, Zougman A, Nagaraj N, Mann M. Universal sample preparation method for proteome analysis. *Nature methods* 2009, **6**(5): 359–362.
78. Wang LH, Li DQ, Fu Y, Wang HP, Zhang JF, Yuan ZF, *et al.* pFind 2.0: a software package for peptide and protein identification via tandem mass spectrometry. *Rapid communications in mass spectrometry: RCM* 2007, **21**(18): 2985–2991.
79. Frokjaer-Jensen C. Exciting prospects for precise engineering of Caenorhabditis elegans genomes with CRISPR/Cas9. *Genetics* 2013, **195**(3): 635–642.
80. Dickinson DJ, Ward JD, Reiner DJ, Goldstein B. Engineering the Caenorhabditis elegans genome using Cas9-triggered homologous recombination. *Nature methods* 2013, **10**(10): 1028–1034.
81. Dokshin GA, Ghanta KS, Piscopo KM, Mello CC. Robust Genome Editing with Short Single-Stranded and Long, Partially Single-Stranded DNA Donors in Caenorhabditis elegans. *Genetics* 2018, **210**(3): 781–787.
82. Kaletsky R, Yao V, Williams A, Runnels AM, Tadych A, Zhou S, *et al.* Transcriptome analysis of adult Caenorhabditis elegans cells reveals tissue-specific gene and isoform expression. *PLoS genetics* 2018, **14**(8): e1007559.
83. Ma J, Chen T, Wu S, Yang C, Bai M, Shu K, *et al.* iProX: an integrated proteome resource. *Nucleic acids research* 2019, **47**(D1): D1211-D1217.
84. Hillers KJ, Jantsch V, Martinez-Perez E, Yanowitz JL. Meiosis. *WormBook: the online review of C elegans biology* 2017, **2017**: 1–43.

Figures

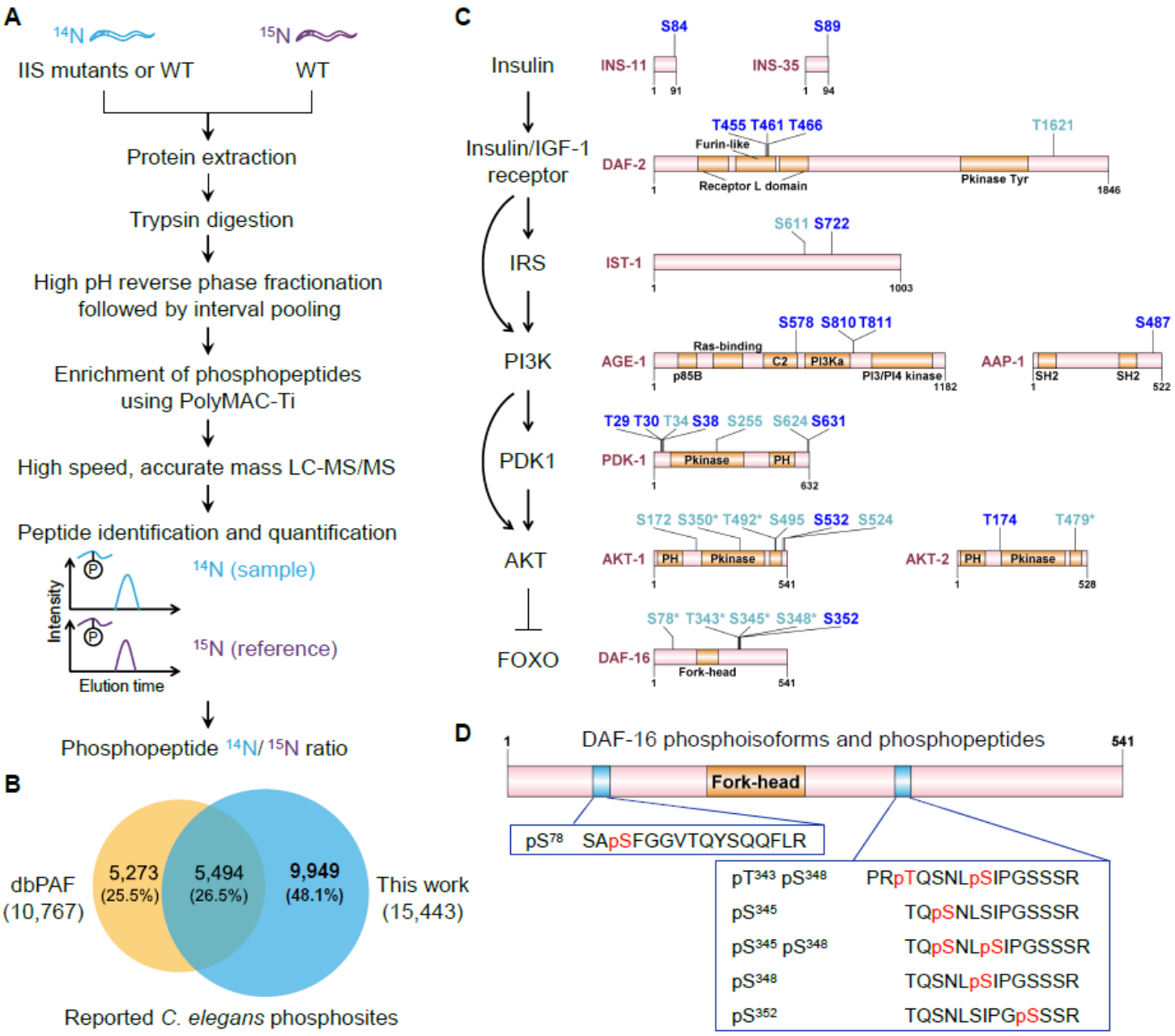

Figure 1

Characterization of the C. elegans Phosphoproteome (A) Phosphoproteomics profiling of wild type (WT) and Insulin/IGF-1 Signaling (IIS) mutants by advanced techniques, including extensive high-pH reverse phase fractionation followed by interval pooling, polyMAC-TiO2 enrichment of phosphopeptides, as well as high-speed, accurate-mass mass spectrometry. Phosphopeptides from synchronized adult day one worms were quantified against a stable-isotope-labeled internal reference (introduced via feeding WT worms entirely on 15N-labeled E. coli cells). (B) The identification scope of this study: 9,949 of the 15,443 high-confidence phosphosites identified here were not present in the latest release of the C. elegans phosphosite database (dbPAF). (C) Phosphorylation of C. elegans IIS proteins. Phosphosites identified in this study are displayed with S or T (serine and threonine), followed by their residue number. Dark blue

highlights the 17 newly identified phosphosites among C. elegans IIS proteins. (D) The DAF-16, isoform h protein, as an example to illustrate phosphoisoforms derived from the identified tryptic phosphopeptides. pT343 pS348 and pS345 pS348 are phosphoisoforms that carry two phosphosites. A phosphorylation hotspot was observed at the C-terminal end of the DAF-16 Forkhead domain. Only pS345 is positioned within a consensus sequence (RPRTQS345) that matches the known AKT-1 phosphorylation consensus motif (RxRxxS/T). See also Supplementary Fig. 1, and Supplementary Table 1.

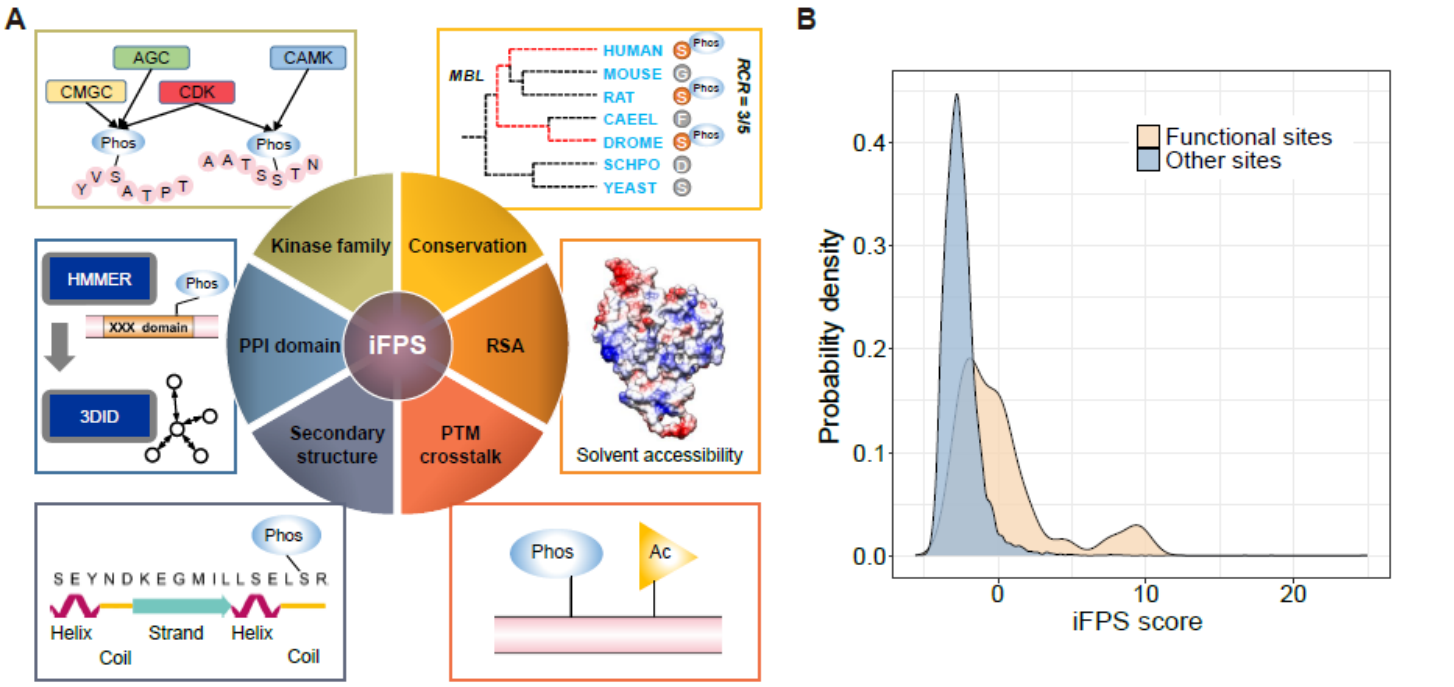

D

Biological function	Protein	Site	Phosphoisoform	*daf-2* /Ctrl*	Protein *daf-2* /WT#
AMPK signaling/ Insulin signaling	AAK-2	T597	pT597 pS601; pT597	1.47; 1.50	2.17
		S601	pT597 pS601	1.47	
		S553	pS553	0.61	
	AKT-1	T492	T492	2.20	2.44
	DAF-16	S345 S348	pS345 pS348	0.25	n.a.
Translation initiation/ Ribosome biogenesis	BYN-1	S46	pS46	1.37	0.86
	DAO-5	S583	pS858 pS861	0.55	0.58
	EGL-45	S978	pS978	0.65	1.05
	EIF-2α	S49	pS49	1.83	0.93
Cell cycle	CDK-1	T32	pT32 pY33	0.76	1.13
		Y33	pT32 pY33; pY33	0.76; 0.51	
		T179	T179	0.60	
	CHK-2	S10 S11	pS10 pS11	0.39	n.a.
	PUF-3	S56	pS56	0.17	n.a.
Zinc metabolism	CDF-1	S324	S324	0.69	n.a.
Intermediate filament	IFA-1	S52	pS49 pS52	0.72	0.56
Clathrin-mediated endocytosis	MLT-3	S252	S252	1.42	1.67
Cholesterol biosynthesis	MVK-1	S252	S252	1.29	1.00
Acetyl-coA biosynthesis	PDHA-1	S287	S287	0.76	0.97
piRNA biogenesis	TOST-1	S94	S94	0.42	0.93
Unknown	CEST-13	S202	S202	2.61	n.a.
	F21F3.2	Y179	pY179	0.57	n.a.
	F36D4.5	S256	S256	0.54	n.a.
	PQN-59	S255	pS253 pS255	0.69	0.74
	T04A8.8	S245	pS245	0.67	0.77

Figure 2

Discerning Functionally Relevant Clues from the Phosphoproteome. (A) Schematic diagram illustrating the design of our newly developed iFPS (Inference of Functional Phosphorylation Sites) algorithm, which

employs multinomial logistic regression from machine learning to integrate six constraints and predict the functionally impactful phosphosites in C. elegans. RSA relative surface accessibility, Phos phosphorylation, Ac acetylation. (B) Distribution of iFPS scores for phosphosites identified in this study. Yellow represents the known functional phosphosites (n = 31), blue represents the rest (n = 15,235). (C) Phosphorylation changes in the long-lived daf-2 mutant. A stringent filter was applied to the data, requiring at least three independent and reliable quantitation measurements in both the daf-2 mutant and a control (WT or WT plus daf-16 mutants, see Methods). In total, 222 down- and 226 up-regulated phosphoisoforms were detected in the daf-2 mutant, including a “strict” subset colored in red (fold change (FC) beyond 1.5 standard deviation (SD) and $p < 0.05$, Wilcoxon rank-sum test) and a “loose” subset colored in yellow (FC beyond 1.5 SD and $p \leq 0.10$ or FC beyond 1.0 SD and $p < 0.05$, Wilcoxon rank-sum test). (D) Prioritizing the daf-2 regulated phosphosites based on iFPS. The daf-2 regulated phosphosites that ranked among the top 5% highest scoring iFPS phosphosites are shown. For each of the three prominent protein function groups, the selected phosphosite (highlighted in red) was functionally validated in the present study. *phosphorylation fold change. #protein fold change (adult day one worm proteomics data, from Walther et al., 20156). See also Supplementary Fig. 2, Supplementary Table 2 and 3.

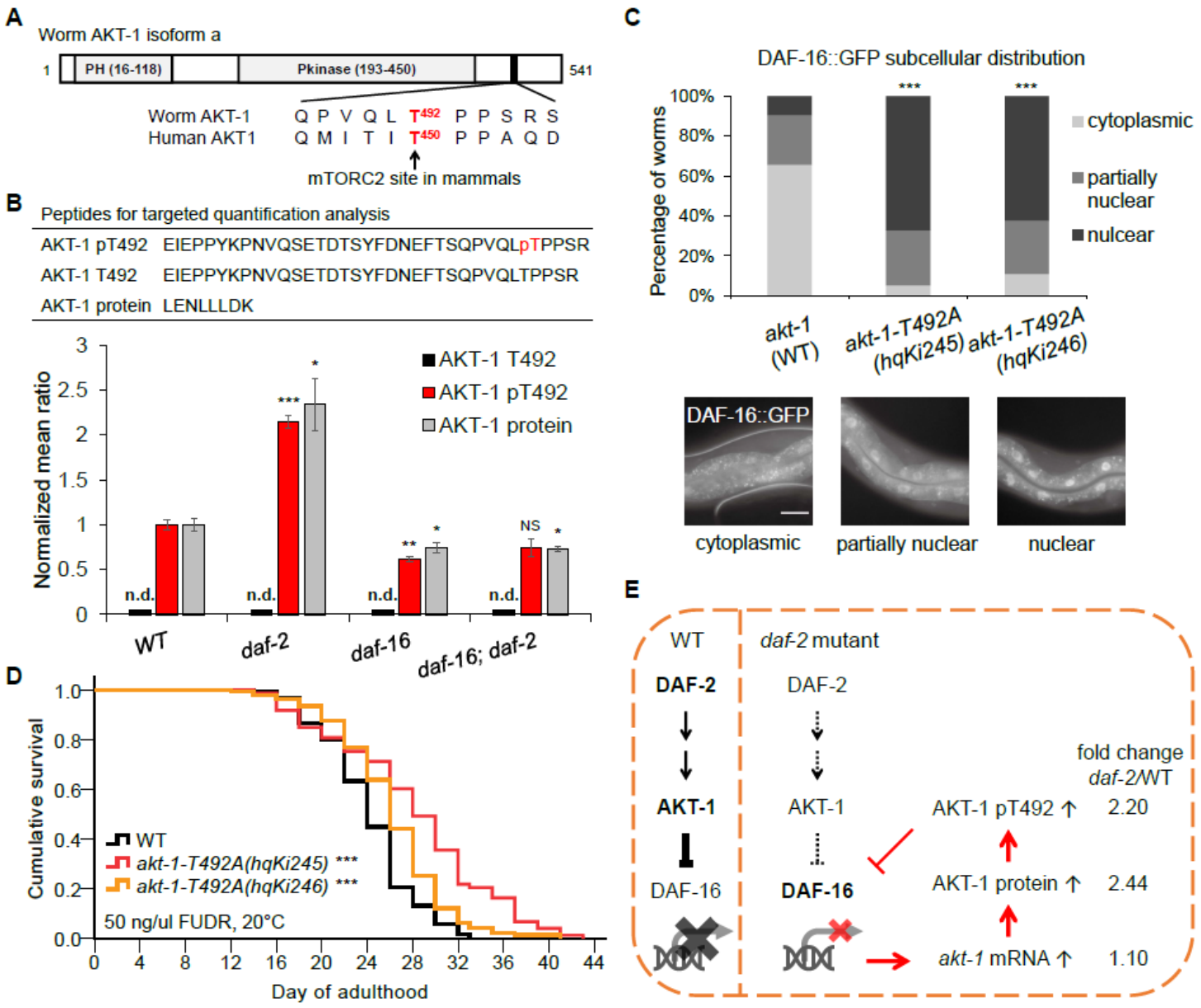

Figure 3

Constitutive Phosphorylation of AKT-1 T492 Compensates for Loss of daf-2 (A) Schematic of the protein structure of worm AKT-1, isoform a. The phosphosite pT492 is conserved with human AKT1 pT450, a known mTORC2 target site. Sequences surrounding the worm AKT-1 T492 and human AKT1 T450 were aligned using a UniProt website tool (https://www.uniprot.org/align/). PH Pleckstrin Homology domain, Pkinase Protein kinase domain. (B) Phosphorylation on AKT-1 T492 is constitutive. MS-based quantification of target peptides (detailed in list) indicating that daf-2 mutation significantly enhanced the levels of both the AKT-1 pT492 and AKT-1 proteins, doing so in a daf-16 dependent manner. In contrast endogenous unphosphorylated AKT-1 T492 peptides were not detected. Target peptides were quantified against isotopically labeled synthetic peptides spiked into whole worm lysates. Mean ratios represent the abundance of target peptides divided by that of cognate labeled peptides. For each target, data from mutant strains were normalized to the mean ratio quantified in WT. n.d. not detected. *p < 0.05,

**p < 0.01, ***p < 0.001, mutant versus WT, Student's t test, error bars denote the SEM. (C) AKT-1 T492A induced nuclear accumulation of DAF-16. Representative images show endogenous DAF-16::GFP cellular localization in intestinal cells at late L4 or early adult day one. hqKi245 and hqKi246 are akt-1-T492A mutants generated using CRISPR/Cas9 technology. ***p < 0.001, mutant versus WT, Fisher exact test. Number of worms counted: 64, 58, and 64 for WT, hqKi245, and hqKi246, respectively. Scale bar: 30 μm. (D) AKT-1 T492A significantly extended the lifespan of C. elegans. ***p < 0.001, log-rank test, n > 70 per strain. (E) A model illustrating the IIS feedback regulation at the AKT-1 level. akt-1 mRNA data, from Son et al., 201733. See also Supplementary Fig. 3, and Supplementary Table 4-5.

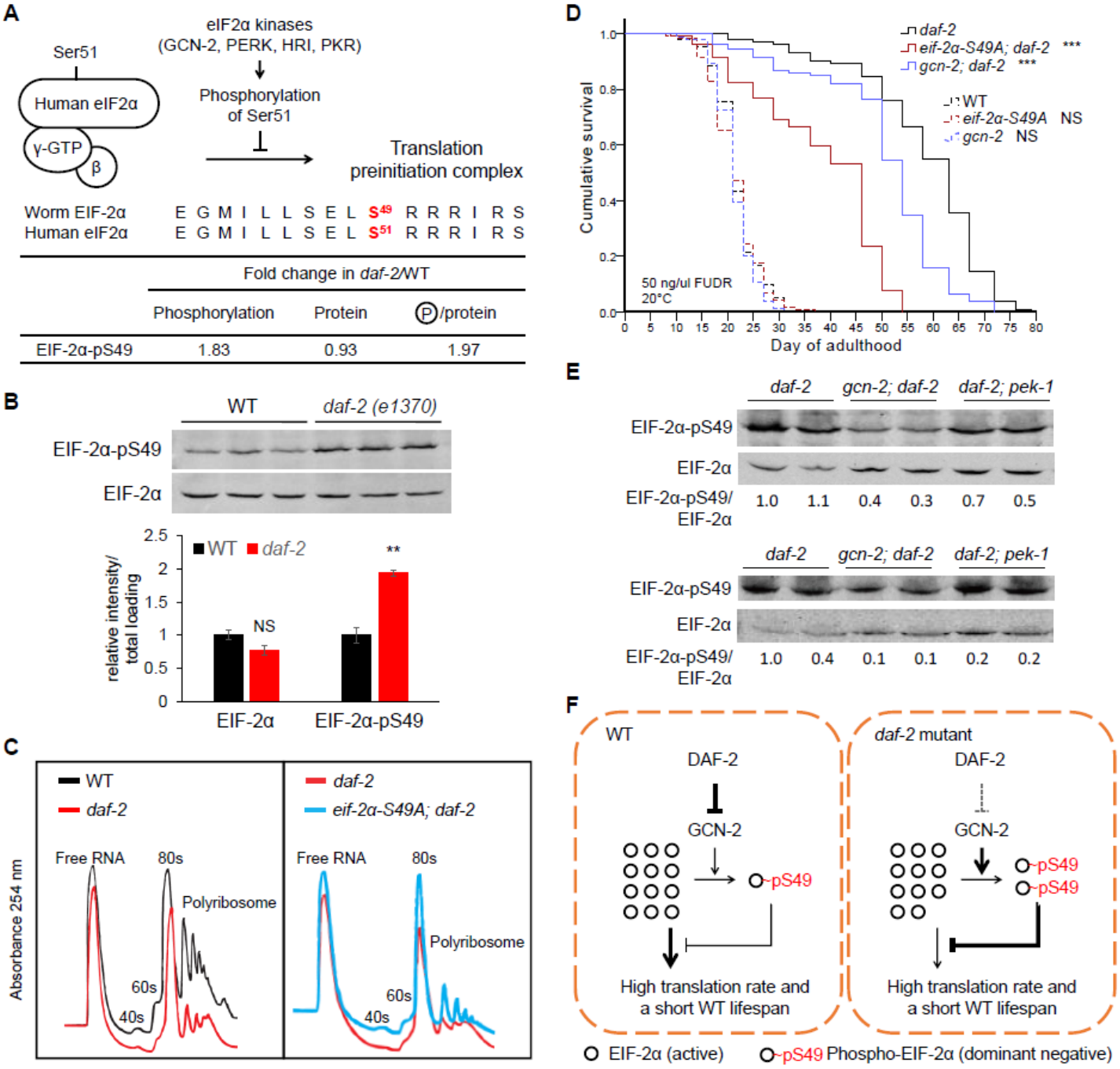

Figure 4

EIF-2α pS49 is a Potent Regulator of Translation and Lifespan in daf-2 (A) Phosphoproteomics data showed that EIF-2α S49, corresponding to human eIF2α S51, is hyper-phosphorylated in the daf-2 mutant. Model illustrating that phosphorylation on the α-subunit of human eIF2 by kinases including GCN-2, PERK, HRI, and PKR prevents the formation of translation preinitiation complex, which results in translational repression of global protein synthesis. (B) Western blotting analysis confirmed that the phosphorylation on EIF-2α S49 was up-regulated in the daf-2(e1370) mutant at adult day one. Immunoblot of WT or daf-2 mutant worm lysates, probed with a phospho-specific antibody that recognizes EIF-2α pS49, or with an antibody specific to the EIF-2α total protein. NS not significant, **p < 0.01, Student's t test, error bars denote the SEM. (C) Polyribosome profiles of the WT, daf-2(e1370), or eif-2α-S49A(hqKi188); daf-2(e1370) worms harvested at adult day one. hqKi188 was generated using CRISPR/Cas9 technology. For each strain, worm lysate samples with the same amount total protein concentration were separated by sucrose gradient centrifugation, and analyzed with the absorbance recording at OD 254 nm. (D) Phosphorylation of EIF-2α S49 contributes significantly to daf-2 longevity. eif-2α-S49A(hqKi188) mutation and EIF-2α kinase mutation gcn-2(ok886) significantly shortened the lifespan of the daf-2(e1370) worms, but did not disturb the WT lifespan. ***p < 0.001, NS not significant, log-rank test, n > 80 per strain. (E) Western blot showing the level of EIF-2α pS49 and EIF-2α total protein in the daf-2(e1370), gcn-2(ok886); daf-2(e1370), or daf-2(e1370); pek-1(ok275) mutants harvested at adult day one. The ratios of EIF-2α pS49 intensity, normalized to the EIF-2α total protein level, are presented below. In both trials, through comparing to daf-2, EIF-2α pS49 was markedly decreased in gcn-2; daf-2 but mildly reduced in daf-2; pek-1. (F) A model illustrating that IIS regulates EIF-2α S49 phosphorylation though GCN-2. EIF-2α pS49 potently inhibit protein synthesis and contributes substantially to daf-2 longevity. See also Supplementary Fig. 4 and Supplementary Table 4.

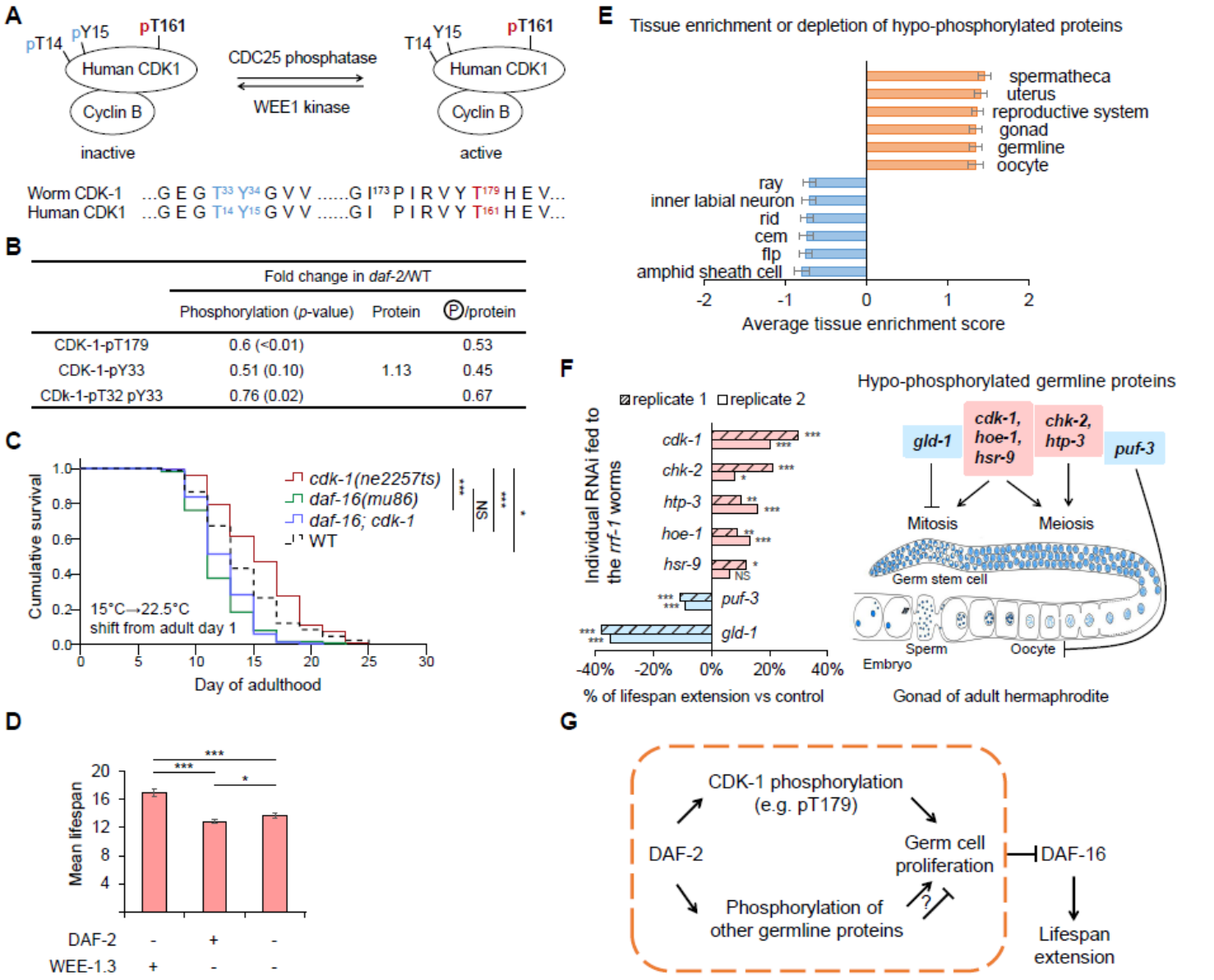

Figure 5

CDK-1 pT179 and Other Germline Phosphoproteins Contribute to Lifespan Determination (A) Model shows the human CDK1 activity regulated through phosphorylation by WEE1 kinase and CDC25 phosphatase. Amio acid sequences around the essential phosphosites on worm CDK-1 (pT32, pY33, and pT179) are identical to human CDK1 (pT14, pY15, and pT161). Blue, inhibitory phosphorylation. Red, activating phosphorylation. (B) Phosphoproteomics data show that the abundance of phosphorylation on CDK-1 decreased in the daf-2 mutant. CDK-1 protein levels remained similar in WT and daf-2 worms. (C) Reduction of CDK-1 activity significantly extended the lifespan of WT worms, but did not affect the lifespan of the daf-16(mu86) worms. The ne2257ts[cdk-1-I173F] mutation inactivates CDK-1 at the restricted temperature 22.5°C. (D) Germline-restricted degradation of WEE-1.3, a negative regulator of CDK-1, significantly shortened the C. elegans lifespan. Endogenous wee-1.3 and daf-2 was tagged with a degron using CRISPR/Cas9. All strains carry the ieSi38[Psun-1::TIR1] allele to induce germline specific

protein degradation in the presence of auxin. Lifespan assays were performed at 20°C, with 1mM auxin supplied from adult day one. (E) Top-ranking six tissues which were significantly ($p < 1.0e-15$, Z-test) enriched or depleted for the hypo-phosphorylated proteins in the daf-2 mutant. Gene expression prediction scores across tissues or cell types were derived from Kaletsky et al., 201882. Error bar represents the SEM. (F) Germline proteins which are hypo-phosphorylated in the daf-2 mutant participate in lifespan regulation. Individual RNAi clone of seven genes was fed to the rrf-1(pk1417) worms from adult day one at 20°C. Genes that regulate germ cell proliferation was based on phenotypic data from WormBase release WS275. The diagram of a gonad was adapted from the meiosis chapter of WormBook84. (G) A model illustrating dual roles of germline phosphoproteins in mediating the effects of IIS on reproduction and lifespan regulation. *$p < 0.05$, **$p < 0.01$, ***$p < 0.001$, NS not significant, log-rank test, $n > 80$ per strain. See also Supplementary Fig. 5 and Supplementary Table 4.

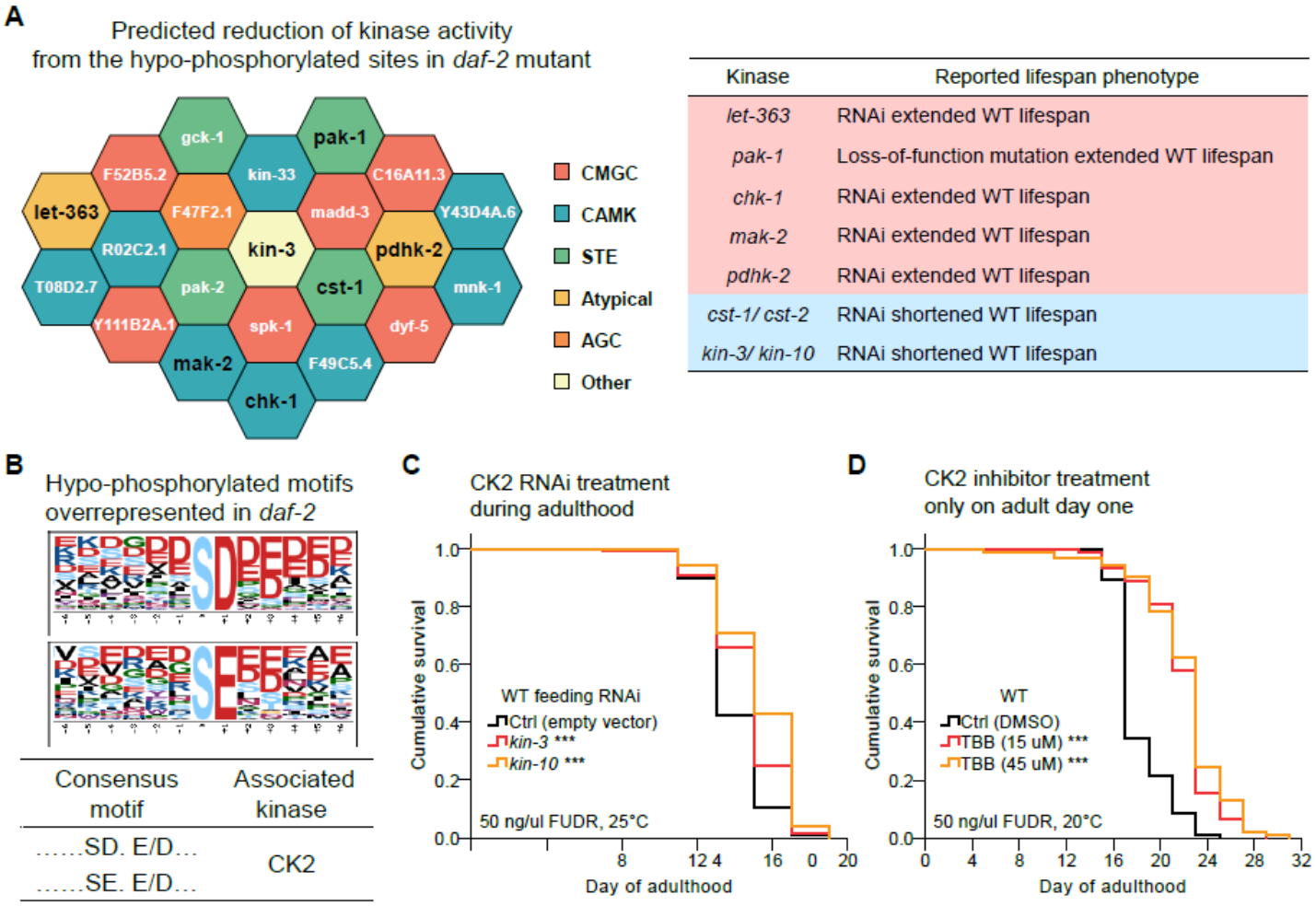

Figure 6

Inhibition of Casein Kinase 2 (CK2) Extends the Worm Lifespan (A) Honeycomb diagram displaying iGPS-predicted kinases whose target motifs were significantly (Benjamini-Hochberg adjustment $p < 0.05$, hypergeometric test) enriched among the hypo-phosphorylated sites in the daf-2 mutant. Kinase groups are depicted in different colors. Bold black highlights the kinases reported to regulate lifespan. Lifespan

data were derived from WormBase. (B) CK2 consensus motifs overrepresented (Motif-X, criteria: significance < 1E-6) in the hypo-phosphorylated peptides in the daf-2 mutant. (C) CK2 knockdown in adulthood significantly extended the lifespan of WT worms. kin-3 or kin-10 encodes the catalytic or regulatory subunit of CK2, respectively. (D) 24-hour treatment of TBB, the highly selective inhibitor of CK2, from adult day one significantly extended the lifespan of C. elegans. *** p-value < 0.001, log-rank test, n > 70 per strain. See also Supplementary Table 4.

daf-2(lf)-induced changes and their effects on lifespan

	Kinome	Negative feedback regulation of IIS	Translation	Reproduction	
	CK2 and other kinases in Fig. 6A	AKT-1	EIF-2α	CDK-1	HOE-1, HSR-9, GLD-1, PUF-3, and more
mRNA	Vary	—	—	—	Vary
Protein	Vary	↑	—	—	Vary
PTM or activity	Activity ↓ (inferred)	AKT-1 pT492 ↑	EIF-2α pS49 ↑	CDK-1 pT179 ↓	Phosphorylation ↓
Effect on lifespan	↑ Lifespan (6/7 kinases)	↓ Lifespan	↑ Lifespan	↑ Lifespan	Negative correlation between effect on reproduction and effect on lifespan
Key regulation		Protein abundance & PTM	PTM	PTM	

Figure 7

Phosphoproteomics Analysis Supports Concerted Regulation of Longevity from Multiple Pathways Upon Reduced IIS daf-2(lf) induced extensive phosphorylation changes on components of the IIS pathway, translational machinery, reproductive system and kinome. Phosphorylation changes at AKT-1 pT492, EIF-2α pS49, and CDK-1 pT179 all affect lifespan, while their parent proteins and the encoding mRNAs show no or little change in the daf-2 mutant, except for AKT-1. The proteins involved in reproduction and lifespan determination are likely regulated through phosphorylation by IIS, since no clear pattern of changes are evident based on analysis of their mRNA or protein levels. Similarly, reduction in IIS may lower the activity of pro-ageing kinases, and the regulation pattern cannot be inferred from mRNA or protein abundance changes. ↑ increase or extend, ↓ decrease or shorten, — no significant change.

Supplementary Files

This is a list of supplementary files associated with this preprint. Click to download.

- SupplementaryInformation.pdf
- SupplementaryTable1.xlsx

- SupplementaryTable2.xlsx
- SupplementaryTable3.xlsx
- SupplementaryTable4.xlsx
- SupplementaryTable5.xlsx